Table 2. Incidence of MSI and LOH in 100 patients with oesophageal cancer

	MSI (1 locus, 2 loci)	Mixed	LOH (1 locus, 2 loci)	Negative	Total
Japanese	4 (8%) (4, 0)	1 (2%)	25 (50%) [12 (24%), 13 (26%)]	21 (42%)	50
Chinese	2 (4%) (1, 1)	2 (4%)	35 (70%) [17 (34%), 18 (36%)]	13 (26%)	50

sensus of investigators who search for LOH using fluorescent systems seems to be that results showing a significant reduction in the signal magnitude of peaks derived from either of the parental alleles can be designated as LOH. If clusters of peaks derived from both alleles are completely separated in an electrophoretogram, designation of LOH is not difficult. However, when both peak clusters are close, the possibility that microsatellite length has simply changed in a the part of tumour cell population cannot be excluded (fig. 1b). This pattern was referred to as an 'ambiguous alteration' in this study. In addition, since every tumour specimen contains many normal cells, including fibroblasts, these changes in the signal magnitude of peaks are modest in many cases. In this study, we defined LOH as a significant reduction ($\geq 30\%$) in the signal magnitude of peaks derived from either of the parental alleles when both paternal and maternal peak clusters are clearly, i.e. over 2 base pairs, separated in an electrophoretogram. This is based on a series of experiments in which reproducibility of the quantitative relationship between paternal and maternal peak clusters was examined in over 20 independent PCR analyses of the same DNA samples. The relative difference of the signal magnitude between paternal and maternal peak clusters did not fluctuate over 10% [unpubl. data]. Such changes will not be detected if a conventional method using radiolabelled PCR and X-ray films is employed. Fluorescent systems have not thus far been used to analyse microsatellite changes in oesophageal cancer. Use of the sensitive and quantitative fluorescent system has led to an efficient discrimination between MSI and LOH, based on quantitative arguments. Nevertheless, some cases have remained as ones with ambiguous alterations. As discussed above, these are theoretically indistinguishable between MSI and LOH. Without the use of different approaches, these patterns cannot be clearly discriminated.

The occurrence of oesophageal cancer differs depending on geographical areas and populations, which implies that specific environmental or genetic factors may underlie tumorigenesis in the oesophagus. The oesophagus, the entrance to the digestive tract, is exposed to a wide variety of chemical substances. Among the risk factors derived from lifestyle, smoking and drinking are known factors. In Barrett's cancer, another type of oesophageal cancer that was not addressed in this study, reflux of gastric juice is considered to be a cause [37]. However, specific environmental substances relevant to an occurrence of squamous cell carcinoma in the oesophagus have not been identified. In colorectal cancer, genetic defects leading to a deficiency in DNA mismatch repair are known to be a risk factor. Indeed, defective mismatch repair is noted not only in kindred of a familial cancer syndrome, HNPCC [1, 2], but also in sporadic cases of colorectal cancer [38–42]. Our data revealed the low incidence of MSI in oesophageal cancer, which implies that loss of DNA mismatch repair is rare, at least in Japanese and Chinese patients with oesophageal cancer. The contribution of defective mismatch repair to tumorigenesis in the oesophagus may be limited. On the other hand, LOH was frequent, which is consistent with data found in the literature [25–31]. Among the five microsatellite markers that we used here, D2S123 and D13S175 had been examined by different groups. Ogasawara et al. [19] reported 3% as the frequency of LOH at the D25/23 locus, while in our study, the rate was higher, i.e. 22% for the both panels. In the region flanking D2S123, the *hMSH2* gene, one of the genes encoding one of the major DNA mismatch repair proteins has been mapped [2, 43]. However, defective mismatch repair as a cause of tumourigenesis is unlikely, as discussed above. The BRCA2 gene is located near the D13S175 locus [28]. BRCA1 and BRCA2 proteins are suggested to function in the recombinational repair pathways in mammalian cells [44, 45]. Harada et al. [28] reported that the frequency of LOH in D13S175 and D13S171 was 10.4 and 38.6%, respectively, and our rates for D13S175 LOH in the two panels were 16 and 26%. Indeed, the region 13q has been reported to be one of the hot spots for LOH in oesophageal cancer [28, 46, 47]. Deletion of specific chromosomal segments and con-

sequent loss of functions in specific genes may relate to tumourigenesis in the oesophagus. In our study, a considerable number of cases showed LOH at more than one locus, and no hot spot was found in the set of five microsatellite markers. This finding may rather suggest that chromosome instability leading to a multicentric loss of chromosome segments may underlie tumourigenesis in the oesophagus. Chromosome instability might be ultimately derived from some environmental substances, as yet unidentified.

In conclusion, in squamous cell carcinoma in the oesophagus, large-scaled chromosomal changes, rather than relatively modest changes such as MSI, are predominant.

Acknowledgement

This study was supported by grants from the Ministry of Education, Science, Sports and Culture of Japan.

References

1 Fishel R, Lescoe MK, Rao MRS, Copeland NG, Jenkins NA, Garber J, Kane M, Kolodner R: The human mutator gene homolog MSH2 and its association with hereditary nonpolyposis colon cancer. Cell 1993; 75: 1027–1038.

2 Leach FS, Nicolaides NC, Papadopoulos N, Liu B, Jen J, Parsons R, Peltomaki P, Sistonen P, Aaltonen LA, Nystrom-Lahti M, Guan X, Zhang J, Meltzer PS, Yu J, Kao F, Chen DJ, Cerosaletti KM, Fournier REK, Todd S, Lewis T, Leach RJ, Naylor SL, Weissenbach J, Mecklin JP, Jarvinen H, Petersen GM, Hamilton SR, Green J, Jass J, Watson P, Lynch HT, Trent JM, de la Chapelle A, Kinzler KW, Vogelstein B: Mutations of a mutS homolog in hereditary nonpolyposis colorectal cancer. Cell 1993; 75: 1215–1225.

3 Gonzalez-Zulueta M, Ruppert JM, Tokino K, Tsai YC, Spruck CH III, Miyao N, Nichols PW, Hermann GG, Horn T, Steven K, Summerhayes IC, Sidransky D, Jones PA: Microsatellite instability in bladder cancer. Cancer Res 1993; 53: 5620–5623.

4 Lothe RA, Peltomaki P, Meling GI, Aaltonen LA, Nystrom-Lahti M, Pylkkanen L, Heimdal K, Andersen TI, Moller P, Rognum TO, Fossa SD, Haldorsen T, Langmark F, Brogger A, de la Chapelle A, Borresen AL: Genomic instability in colorectal cancer: Relationship to clinicopathological variables and family history. Cancer Res 1993; 53: 5849–5852.

5 Risinger JI, Berchuck A, Kohler MF, Watson P, Lynch HT, Boyd J: Genetic instability of microsatellites in endometrial carcinoma. Cancer Res 1993; 53: 5100–5103.

6 Thibodeau SN, Bren G, Schaid D: Microsatellite instability in cancer of the proximal colon. Science 1993; 260: 816–819.

7 Ribeiro U Jr, Posner MC, Safatle-Ribeiro AV, Reynolds JC: Risk factors for squamous cell carcinoma of the oesophagus. Br J Surg 1996; 83: 1174–1185.

8 Field JK, Kiaris H, Howard P, Vaughan ED, Spandidos DA, Jones AS: Microsatellite instability in squamous cell carcinoma of the head and neck. Br J Cancer 1995; 71: 1065–1069.

9 Gleeson CM, Sloan JM, McGuigan JA, Ritchie AJ, Weber JL, Russell SEH: Ubiquitous somatic alterations at microsatellite alleles occur infrequently in Barrett's-associated esophageal adenocarcinoma. Cancer Res 1996; 56: 259–263.

10 Gleeson CM, Sloan JM, McGuigan JA, Ritchie AJ, Weber JL, Russell SEH: Barrett's oesophagus: Microsatellite analysis provides evidence to support the proposed metaplasia-dysplasia-carcinoma sequence. Genes Chromosomes Cancer 1998; 21: 49–60.

11 Hibi K, Kondo K, Akiyama S, Ito K, Takagi H: Frequent genetic instability in small intestinal carcinomas. Jpn J Cancer Res 1995; 86: 357–360.

12 Ikeguchi M, Unate H, Maeta M, Kaibara N: Detection of loss of heterozygosity at microsatellite loci in esophageal squamous-cell carcinoma. Oncology 1999; 56: 164–168.

13 Iwaya T, Maesawa C, Nishizuka S, Suzuki Y, Sakata K, Sato N, Ikeda K, Koeda K, Ogasawara S, Otsuka K, Kimura Y, Aoki K, Ishida K, Saito K, Tamura G: Infrequent frameshift mutations of polynucleotide repeats in multiple primary cancers affecting the esophagus and other organs. Genes Chromosomes Cancer 1998; 23: 317–322.

14 Keller G, Rotter M, Vogelsang H, Bischoff P, Becker KF, Mueller J, Brauch H, Siewert JR, Hofler H: Microsatellite instability in adenocarcinomas of the upper gastrointestinal tract. Relation to clinicopathological data and family history. Am J Pathol 1995; 147: 593–600.

15 Meltzer SJ, Yin J, Manin B, Rhyu M, Cottrell J, Hudson E, Redd JL, Krasna MJ, Abraham JM, Reid BJ: Microsatellite instability occurs frequently and in both diploid and aneuploid cell populations of Barrett's-associated esophageal adenocarcinomas. Cancer Res 1994; 54: 3379–3382.

16 Mironov NM, Aguelon AM, Hollams E, Lozano JC, Yamasaki H: Microsatellite alterations in human and rat esophageal tumors at selective loci. Mol Carcinog 1995; 13: 1–5.

17 Muzeau F, Flejou JF, Belghiti J, Thomas G, Hamelin R: Infrequent microsatellite instability in oesophageal cancers. Br J Cancer 1997; 75: 1336–1339.

18 Nakashima H, Mori M, Mimori K, Inoue H, Shibuta K, Baba K, Mafune K, Akiyoshi T: Microsatellite instability in Japanese esophageal carcinoma. Int J Cancer 1995; 64: 286–289.

19 Ogasawara S, Maesawa C, Tamura G, Satodate R: Frequent microsatellite alterations on chromosome 3p in esophageal squamous cell carcinoma. Cancer Res 1995; 55: 891–894.

20 Shimada M, Horii A, Sasaki S, Yanagisawa A, Kato Y, Yamashita K, Okagawa K, Yamasaki K, Ishiguro S, Inoue M, Shiozaki H, Nakamura Y: Infrequent replication errors at microsatellite loci in tumors of patients with multiple primary cancers of the esophagus and various other tissues. Jpn J Cancer Res 1995; 86: 511–515.

21 Wu T, Watanabe T, Heitmiller R, Zahurak M, Forastiere AA, Hamilton SR: Genetic alterations in Barrett esophagus and adenocarcinomas of the esophagus and esophagogastric junction region. Am J Pathol 1998; 153: 287–294.

22 Arzimanoglou II, Gilbert F, Barber HRK: Microsatellite instability in human solid tumors. Cancer 1998; 82: 1808–1820.

23 Claij N, te Riele H: Microsatellite instability in human cancer: A prognostic marker for chemotherapy? Exp Cell Res 1999; 246: 1–10.

24 Ruschoff J, Bocker T, Schlegel J, Stumm G, Hofstaedter F: Microsatellite instability: New aspects in the carcinogenesis of colorectal carcinoma. Virchows Arch 1995; 426: 215–222.

25 Aoki T, Mori T, Du X, Nisihira T, Matsubara T, Nakamura Y: Allelotype study of esophageal carcinoma. Genes Chromosomes Cancer 1994; 10: 177–182.

26 Barrett MT, Galipeau PC, Sanchez CA, Emond MJ, Reid BJ: Determination of the frequency of loss of heterozygosity in esophageal adenocarcinoma by cell sorting, whole genome amplification and microsatellite polymorphisms. Oncogene 1996; 12: 1873–1878.

▶27 Boynton RF, Blount PL, Yin J, Brown VL, Huang Y, Tong Y, McDaniel T, Newkirk C, Resau JH, Raskind WH, Haggitt RC, Reid BJ, Meltzer SJ: Loss of heterozygosity involving the APC and MCC genetic loci occurs in the majority of human esophageal cancers. Proc Natl Acad Sci USA 1992; 89: 3385–3388.

▶28 Harada H, Tanaka H, Shimada Y, Shinoda M, Imamura M, Ishizaki K: Lymph node metastasis is associated with allelic loss on chromosome 13q12–13 in esophageal squamous cell carcinoma. Cancer Res 1999; 59: 3724–3729.

▶29 Moskaluk CA, Rumpel CA: Allelic deletion in 11p15 is a common occurrence in esophageal and gastric adenocarcinoma. Cancer 1998; 83: 232–239.

▶30 Ogasawara S, Tamura G, Maesawa C, Suzuki Y, Ishida K, Satoh N, Uesugi N, Saito K, Satodate R: Common deleted region on the long arm of chromosome 5 in esophageal carcinoma. Gastroenterology 1996; 110: 52–57.

▶31 Shibagaki I, Shimada Y, Wagata T, Ikenaga M, Imamura M, Ishizaki K: Allelotype analysis of esophageal squamous cell carcinoma. Cancer Res 1994; 54: 2996–3000.

▶32 Boland CR, Thibodeau SN, Hamilton SR, Sidransky D, Eshleman JR, Burt RW, Meltzer SJ, Rodriguez-Bigas MA, Fodde R, Ranzani GN, Srivastava S: A National Cancer Institute Workshop on Microsatellite Instability for cancer detection and familial predisposition: Development of international criteria for the determination of microsatellite instability in colorectal cancer. Cancer Res 1998; 58: 5248–5257.

▶33 Oda S, Oki E, Machara Y, Sugimachi K: Precise assessment of microsatellite instability using high resolution fluorescent microsatellite analysis. Nucleic Acids Res 1997; 25: 3415–3420.

▶34 Tokunaga E, Oki E, Oda S, Kataoka A, Kitamura K, Ohno S, Machara Y, Sugimachi K: Frequency of microsatellite instability in breast cancer determined by high-resolution fluorescent microsatellite analysis. Oncology 2000; 59: 44–49.

▶35 Ikeda Y, Oda S, Abe T, Ohno S, Machara Y, Sugimachi K: Features of microsatellite instability in colorectal cancer: Comparison between colon and rectum. Oncology 2001; 61: 168–174.

▶36 Machara Y, Oda S, Sugimachi K: The instability within: Problems in current analyses of microsatellite instability. Mutat Res 2001; 461: 249–263.

▶37 Polkowski W, van Lanschot JJB, Offerhaus GJA: Barrett esophagus and cancer: Pathogenesis, carcinogenesis, and diagnostic dilemmas. Histol Histopathol 1999; 14: 927–944.

▶38 Herfarth KKF, Kodner IJ, Whelan AJ, Ivanovich JL, Bracamontes JR, Wells SA Jr, Goodfellow PJ: Mutations in MLH1 are more frequent than in MSH2 in sporadic colorectal cancers with microsatellite instability. Genes Chromosomes Cancer 1997; 18: 42–49.

▶39 Konishi M, Kikuchi-Yanoshita R, Tanaka K, Muraoka M, Onda A, Okumura Y, Kishi N, Iwama T, Mori T, Koike M, Ushio K, Chiba M, Nomizu S, Konishi F, Utsunomiya J, Miyaki M: Molecular nature of colon tumors in hereditary nonpolyposis colon cancer, familial polyposis, and sporadic colon cancer. Gastroenterology 1996; 111: 307–317.

▶40 Kowalski LD, Mutch DG, Herzog TJ, Rader JS, Goodfellow PJ: Mutational analysis of MLH1 and MSH2 in 25 prospectively-acquired RER+ endometrial cancers. Genes Chromosomes Cancer 1997; 18: 219–227.

▶41 Thibodeau SN, French AJ, Roche PC, Cunningham JM, Tester DJ, Lindor NM, Moslein G, Baker SM, Liskay RM, Burgart LJ, Honchel R, Halling KC: Altered expression of hMSH2 and hMLH1 in tumors with microsatellite instability and genetic alterations in mismatch repair genes. Cancer Res 1996; 56: 4836–4840.

▶42 Wu Y, Nystrom-Lahti M, Osinga J, Looman MWG, Peltomaki P, Aaltonen LA, de la Chapelle A, Hofstra RMW, Buys CHCM: MSH2 and MLH1 mutations in sporadic replication error-positive colorectal carcinoma as assessed by two-dimensional DNA electrophoresis. Genes Chromosomes Cancer 1997; 18: 269–278.

▶43 Peltomaki P, Aaltonen LA, Sistonen P, Pylkkanen L, Mecklin JP, Jarvinen H, Green JS, Jass JR, Weber JL, Leach FS, Petersen GM, Hamilton SR, de la Chapelle A, Vogelstein B: Genetic mapping of a locus predisposing to human colorectal cancer. Science 1993; 260: 810–812.

▶44 Morimatsu M, Donoho G, Hasty P: Cells deleted for Brca2 COOH terminus exhibit hypersensitivity to gamma-radiation and premature senescence. Cancer Res 1998; 58: 3441–3447.

▶45 Thompson LH, Schild D: The contribution of homologous recombination in preserving genome integrity in mammalian cells. Biochimie 1999; 81: 87–105.

▶46 Field JK: Genomic instability in squamous cell carcinoma of the head and neck. Anticancer Res 1996; 16: 2421–2431.

▶47 Yoo GH, Xu H, Brennan JA, Westra W, Hruban RH, Koch W, Benedict WF, Sidransky D: Infrequent inactivation of the retinoblastoma gene despite frequent loss of chromosome 13q in head and neck squamous cell carcinoma. Cancer Res 1994; 54: 4603–4606.

Novel SN-38–Incorporating Polymeric Micelles, NK012, Eradicate Vascular Endothelial Growth Factor–Secreting Bulky Tumors

Fumiaki Koizumi,[1] Masayuki Kitagawa,[2] Takahito Negishi,[1] Takeshi Onda,[2] Shin-ichi Matsumoto,[2] Tetsuya Hamaguchi,[3] and Yasuhiro Matsumura[1]

[1]Investigative Treatment Division, Research Center for Innovative Oncology, National Cancer Center Hospital East, Kashiwa, Chiba, Japan; [2]Pharmaceutical Research Laboratories, Research and Development Group, Nippon Kayaku Co., Ltd, Kita-ku, Tokyo, Japan; and [3]Department of Medicine, National Cancer Center Hospital, Tyuo-ku, Tokyo, Japan

Abstract

7-Ethyl-10-hydroxy-camptothecin (SN-38), a biological active metabolite of irinotecan hydrochloride (CPT-11), has potent antitumor activity but has not been used clinically because it is a water-insoluble drug. For delivery by i.v. injection, we have successfully developed NK012, a SN-38-releasing nanodevice. The purpose of this study is to investigate the pharmacologic character of NK012 as an anticancer agent, especially in a vascular endothelial growth factor (VEGF)–secreting tumor model. The particle size of NK012 was ~20 nm with a narrow size distribution. NK012 exhibited a much higher cytotoxic effect against lung and colon cancer cell lines as compared with CPT-11. NK012 showed significantly potent antitumor activity against a human colorectal cancer HT-29 xenograft as compared with CPT-11. Enhanced and prolonged distribution of free SN-38 in the tumor was observed after the injection of NK012. NK012 also had significant antitumor activity against bulky SBC-3/Neo (1,533.1 ± 1,204.7 mm^3) and SBC-3/VEGF tumors (1,620.7 ± 834.0 mm^3) compared with CPT-11. Furthermore, NK012 eradicated bulky SBC-3/VEGF tumors in all mice but did not eradicate SBC-3/Neo tumors. In the drug distribution analysis, an increased accumulation of SN-38 in SBC-3/VEGF tumors was observed as compared with that in SBC-3/Neo tumors. NK012 markedly enhanced the antitumor activity of SN-38, especially in highly VEGF-secreting tumors, and could be a promising SN-38-based formulation. (Cancer Res 2006; 66(20): 10048-56)

Introduction

The antitumor plant alkaloid camptothecin (CPT) is a broad-spectrum anticancer agent that targets DNA topoisomerase I. Although CPT has shown promising antitumor activity *in vitro* and *in vivo* (1, 2), it has not been clinically used because of its low therapeutic efficacy and severe toxicity (3, 4). Among CPT analogues, irinotecan hydrochloride (CPT-11) has recently been shown to be active against colorectal, lung, and ovarian cancer (5–9). CPT-11 itself is a prodrug and is converted to 7-ethyl-10-hydroxy-CPT (SN-38), a biologically active metabolite of CPT-11, by carboxylesterases. SN-38 exhibits up to 1,000-fold more potent cytotoxic activity against various cancer cells *in vitro* than CPT-11 (10). Although CPT-11 is converted to SN-38 in the liver and tumor, the metabolic conversion rate is <10% of the original volume of CPT-11 (11, 12). In addition, the conversion of CPT-11 to SN-38 depends on the genetic interindividual variability of carboxylesterase activity (13). Thus, direct use of SN-38 might be of great advantage and attractive for cancer treatment. For the clinical use of SN-38, however, it is essential to develop a soluble form of water-insoluble SN-38. The progress of the manufacturing technology of "micellar nanoparticles" may make it possible to use SN-38 for *in vivo* experiments and further clinical use.

Passive targeting of drug delivery system is based on the pathophysiologic characteristics that are observed in many solid tumors: hypervascularity, irregular vascular architecture, potential for secretion of vascular permeability factors, and the absence of effective lymphatic drainage that prevents efficient clearance of macromolecules. These characteristics, unique to solid tumors, are believed to be the basis of the enhanced permeability and retention effect (14–17). Supramolecular structures, such as liposomes and polymeric micelles, are expected to increase the accumulation of drugs in tumor tissue through these pathophysiologic features. Polymeric micelle–based anticancer drugs have been developed in recent years (18–20), and some of them have been under evaluation for clinical trials (21–23). This carrier system can incorporate various kinds of drugs into the inner core by chemical conjugation or physical entrapment with relatively high stability, and the size can be controlled within the range of 20 to 100 nm in diameter. This range of diameters is too large to pass through normal vessel walls; therefore, the drug can be expected to reduce side effects due to a decrease in volume of distribution.

Angiogenesis is essential for the growth and metastasis of solid tumors (24). The clinical importance of angiogenesis in human tumors was shown by several reports indicating a positive relationship between the blood vessel density in the tumor mass and poor prognosis for survival in patients with various types of cancers (25–28). Furthermore, Natsume et al. (29) reported that the antitumor activities of anticancer agents, including *cis*-diammine-dichloroplatinum, vincristine, and docetaxel, were less active against vascular endothelial growth factor (VEGF)–secreting cells, SBC-3/VEGF, *in vivo* as compared with its mock transfectant (SBC-3/Neo), although the high vascularity should have been favorable for the drug delivery.

VEGF is also well known as a potent vascular permeability factor (30). The ability of supramolecular structures to accumulate in target tissue is based on the enhanced tumor angiogenesis and tumor vascular permeability that occur in solid tumors. Therefore, we hypothesized that a polymeric micelle–based drug carrier would increase its accumulation and deliver enhanced therapeutic efficacy in tumors that secrete higher levels of VEGF. In the present study, we present the superiority of NK012 over CPT-11 in a tumor model,

Requests for reprints: Yasuhiro Matsumura, Investigative Treatment Division, Research Center for Innovative Oncology, National Cancer Center Hospital East, 6-5-1 Kashiwanoha, Kashiwa, Chiba 277-8577, Japan. Phone: 81-4-7134-6857; Fax: 81-4-7134-6857; E-mail: yhmatsum@east.ncc.go.jp.

doi:10.1158/0008-5472.CAN-06-1605

especially in a VEGF-secreting tumor, and we illustrate the outstanding advantage of polymeric micelle–based drug carriers.

Materials and Methods

Drugs and Cells

SN-38 was synthesized by Nippon Kayaku Co., Ltd. (Tokyo, Japan). CPT-11 was purchased from Yakult Honsha Co., Ltd. (Tokyo, Japan). Human colon cancer cell lines WiDR, SW480, Lovo, and HT-29 and human non–small-cell lung cancer cell line A431 were purchased from American Type Culture Collection (Rockville, MD). Human small-cell lung cancer cell line SBC-3 and human non–small-cell lung cancer cell line PC-14 were kindly provided by Dr. I. Kimura (Okayama University, Okayama, Japan) and Dr. Y. Hayata (Tokyo Medical University, Tokyo, Japan), respectively. SBC-3 and PC-14 were maintained in RPMI 1640 supplemented with 10% fetal bovine serum (Cell Culture Technologies, Gaggenau-Hoerden, Germany), penicillin, streptomycin, and amphotericin B (100 units/mL, 100 μg/mL, and 25 μg/mL, respectively; Sigma, St. Louis, MO) in a humidified atmosphere of 5% CO_2 at 37°C. Other cell lines were maintained in DMEM (Nikken Bio Med. Lab., Kyoto, Japan) supplemented with 10% fetal bovine serum. SBC-3/Neo and SBC-3/VEGF were generated from SBC-3 cells that were transfected with BMG-Neo and BMG-Neo-VEGF as previously reported (29). The full-length sequence of human VEGF expressing 206 amino acids (31) was selected. SBC-3/VEGF cells express ~100 times more soluble VEGF than SBC-3/Neo and SBC-3 cells in the supernatant of cultured cells as shown by ELISA (29).

Preparation of an SN-38–Conjugated Poly(Ethylene Glycol)-Poly(Glutamic Acid) Block Copolymer for NK012 Construction

Poly(ethylene glycol)-poly(glutamic acid) block copolymer [PEG-PGlu(SN-38)] was synthesized as follows: A poly(ethylene glycol)-poly(glutamic acid) block copolymer [PEG-PGlu] was prepared according to the previously reported technique (32, 33). SN-38 was covalently introduced into the PGlu segment by the condensation reaction between the carboxylic acid on PGlu and the phenol on SN-38 with 1,3-diisopropylcarbodiimide and *N,N*-dimethylaminopyridine at 26°C. Consequently, the PGlu segment obtained sufficient hydrophobicity. Accordingly, NK012 was constructed with self-assembling PEG-PGlu(SN-38) amphiphilic block copolymers in an aqueous milieu.

Determination of the Size Distribution of NK012 and Drug Release Behavior of SN-38 from NK012

The size distribution of NK012 was measured with the dynamic light scattering method at 25°C using a Particle Sizer NICOMP 380ZLS (Particle Sizing Systems, Santa Barbara, CA). The release behavior of SN-38 from NK012 was investigated *in vitro* at 20°C or 37°C in PBS (pH 7.3) or 5% glucose solution (pH 4.6). The concentration was 0.1 mg/mL. The amount of SN-38 released from NK012 was estimated by UV measurement at 265 nm.

In vitro Growth Inhibition Assay

The growth inhibitory effects of NK012, SN-38, and CPT-11 were examined with a 3-(4,5-dimethylthiazol-2-yl)-2,5-diphenyltetrazolium bromide (MTT) assay. One hundred eighty microliters of an exponentially growing cell suspension (6×10^3/mL-12×10^3/mL) were seeded into a 96-well microtiter plate, and 20 μL of various concentrations of each drug were added. After incubation for 72 hours at 37°C, 20 μL of MTT solution (5 mg/mL in PBS) were added to each well and the plates were incubated for an additional 4 hours at 37°C. After centrifuging the plates at 200 × *g* for 5 minutes, the medium was aspirated from each well, and 180 μL of DMSO were added to each well to dissolve the formazan. The growth inhibitory effect of each drug was assessed spectrophotometrically (SpectraMax 190, Molecular Devices Corp., Sunnyvale, CA).

In vivo Growth Inhibition Assay

The animal experimental protocols were approved by the Committee for Ethics of Animal Experimentation and the experiments were conducted in accordance with the Guidelines for Animal Experiments in the National Cancer Center or Nippon Kayaku.

Experiment 1. Female BALB/c nude mice, 7 weeks old, were purchased from CLEA Japan (Tokyo, Japan). Human colorectal cancer HT-29 cells were grown as s.c. tumor in the flank of the mice. The tumors were excised from the mice and fragments were inoculated s.c. in the mouse flank. When the tumor volume reached 70 to 170 mm^3, mice were randomly divided into test groups consisting of six mice per group (day 0). Drugs were administered on days 0, 4, and 8 by i.v. injection into the tail vein. NK012 was given at doses of 30 (maximum tolerated dose), 15, and 7.5 mg/kg/d. The reference drug, CPT-11, was given at the maximum tolerated dose, 66.7 mg/kg/d, in the optimal schedule reported (34). The length (a) and width (b) of the tumor mass were measured twice a week, and the tumor volume (TV) was calculated as follows: $TV = (a \times b^2) / 2$. Relative tumor volumes at day n were calculated according to the following formula: $RTV = TV_n / TV_0$, where TV_n is the tumor volume at day n, and TV_0 is the tumor volume at day 0. Differences in relative tumor sizes between the treatment groups at day 21 were analyzed with an unpaired t test.

Experiment 2. As a hypervascular tumor model, we used SBC-3/VEGF cells. SBC-3/Neo or SBC-3/VEGF cells (10^7) were s.c. injected into the back of mice. NK012 or CPT-11 was administered when the mean tumor volumes ($n = 4$) reached a massive size of 1,500 mm^3, which gave tumors almost 1.5 cm in length. It took ~65 days for SBC-3/Neo and 20 days for SBC-3/VEGF to reach the tumor volume of 1,500 mm^3 from the day of inoculation. NK012 at a dose of 10 or 20 mg/kg/d and CPT-11 at a dose of 15 or 30 mg/kg/d were administered i.v. on days 0, 4, and 8. Differences in tumor sizes between the treatment groups and control group at day 14 were analyzed with an unpaired t test.

Histologic and Immunohistochemical Analysis

Histologic sections were taken from SBC-3/Neo and SBC-3/VEGF tumor tissues when the volumes reached 1,500 mm^3. After extirpation, tissues were fixed with 3.9% formalin in PBS (pH 7.4), and the subsequent preparations and H&E staining were done by Tokyo Histopathologic Laboratory Co., Ltd. (Tokyo, Japan). For detection of tumor blood vessels, polyclonal anti–von Willebrand factor antibody (Dako, Glostrup, Denmark) was used.

Assay for SN-38 and CPT-11 in Plasma and Tissues

Female BALB/c nude mice bearing HT-29 (as mentioned in experiment 1; $n = 3$) were used for the analysis of the biodistribution of NK012 and CPT-11. NK012 (30 mg/kg) or CPT-11 (66.7 mg/kg) was administered i.v. to the mice. Under anesthesia, blood and tumor samples were taken at 5 minutes, 1, 6, 24, 48, 72, and 168 hours after administration of NK012 and at 5 minutes, 1, 3, 6, and 24 hours after administration of CPT-11. The blood samples were collected in microtubes and immediately centrifuged at 1,600 × *g* for 15 minutes. The plasma and tumor samples were stored at −80°C until analysis.

For the biodistribution study in hypervascular tumors (experiment 2), female BALB/c nude mice ($n = 3$) bearing 1,500-mm^3 massive SBC-3/Neo and SBC-3/VEGF tumors were used. NK012 (20 mg/kg) and CPT-11 (30 mg/kg) were administered on day 0. The mice were sacrificed at 1, 6, 24, and 72 hours (day 3) after administration. The tumor, liver, spleen, upper small intestine, lung, and blood were taken and stored at −80°C until analysis.

Preparation of the free SN-38 (polymer-unbound SN-38) and CPT-11. Tumor samples were homogenized on ice using a Digital homogenizer (Iuchi, Osaka, Japan) and suspended in the mixture of 100 mmol/L glycine-HCl buffer (pH 3)/methanol (1:1, v/v) at a concentration of 5% w/w. The concentrations of free SN-38 and CPT-11 in the plasma and tumor from aliquots of the homogenates (100 μL) and plasma (50 μL) were determined by high-performance liquid chromatography. For free SN-38 (polymer-unbound SN-38) and CPT-11, proteins were precipitated with an ice-cold mixture of methanol/H_2O/$HClO_4$ (50:45:5, v/v/v) containing CPT as an internal standard. The sample was vortexed for 10 seconds, filtered through a MultiScreen Solvinert (Millipore Corp., Bedford, MA), and analyzed.

Preparation of the polymer-bound SN-38 (SN-38 remaining bound to PEG-PGlu). To permit complete release of SN-38 from the conjugate, 20 μL of plasma and 100 μL of tissue samples were diluted with 20 μL of methanol (50%, v/v) and 20 μL of NaOH (0.3 mol/L for plasma and 0.7 mol/L for tissue). The samples were incubated for 15 minutes at 25°C. After incubation, 20 μL of HCl (0.3 mol/L for plasma and 0.7 mol/L for tissue) and 60 μL of internal standard solution were added to the samples, and then the hydrolysis was filtered through a MultiScreen Solvinert. The filtrate was applied to the high-performance liquid chromatography system.

High-performance liquid chromatography. Reversed-phase high-performance liquid chromatography was done at 35°C on a Mightysil RP-18 GP column 150 × 4.6 mm (Kanto Chemical Co., Inc., Tokyo, Japan). The samples were injected into an Alliance Waters 2795 high-performance liquid chromatography system (Waters, Milford, MA) equipped with a Waters 2475 multi λ fluorescence detector. The detector was set at 365 and 430 nm (excitation and emission, respectively) for CPT-11 and CPT, and at 365 and 540 nm for SN-38. A reversed-phase column was used at 35°C. The mobile phase was a mixture of 100 mmol/L ammonium acetate (pH 4.2) and methanol [11:9 (v/v) for SN-38 in plasma and tumor, 3:2 (v/v) for CPT-11 in plasma, and 63:37 (v/v) for CPT-11 in tumor]. The flow rate was 1.0 mL/min. Peak data were recorded with a chromatography management system (Empower, Waters). Polymer-bound SN-38 was determined by subtraction of polymer-unbound SN-38 from the total SN-38 of the hydrolysate.

Pharmacokinetic and Statistical Analyses

The concentrations of SN-38 and CPT-11 in plasma and tissue were fitted to a pharmacokinetic model by the nonlinear least-square method using WinNonlin Professional software (version 4.1; Pharsight Corp., Palo Alto, CA). We used a noncompartmental analysis. The pharmacokinetic variables were calculated using the following equations (AUC_{last} was calculated by the trapezoidal rule to the last measurable data point):

$$AUC_{inf.} = \int_0^{\infty} C(t)dt$$

$$T_{1/2z}(\text{terminal half} - \text{life}) = 0.693/\lambda z$$

(λz is first-order rate constant associated with the terminal portion of the curve)

$$CL_{tot} = \text{Dose}/AUC_{inf.}$$

$$V_{ss} = \text{MRT} \times CL_{tot}(\text{MRT}, \text{mean residence time})$$

Data were expressed as mean ± SD. Data were analyzed with the Student's t test when the groups showed equal variances (F test) or with Welch's test when they showed unequal variances (F test). $P < 0.05$ was regarded as statistically significant. All statistical tests were two sided.

Results

Preparation and characterization of NK012. NK012 is an SN-38-loaded polymeric micelle constructed in an aqueous milieu by the self-assembly of an amphiphilic block copolymers, PEG-PGlu(SN-38). The molecular weight of PEG-PGlu(SN-38) was determined to be ~19,000 (PEG segment, 12,000; SN-38-conjugated PGlu segment, 7,000). NK012 was obtained as a freeze-dried formulation and contained ca. 20% (w/w) of SN-38 (Fig. 1*A*). The mean particle size of NK012 is 20 nm in diameter with a relatively narrow range (Fig. 1*B*). The releasing rates of SN-38 from NK012 in PBS at 37°C were 57% and 74% at 24 and 48 hours, respectively, and those in 5% glucose solution at 37°C were 1% and 3% at 24 and 48 hours, respectively (Fig. 1*C*). SN-38 is loaded by chemical bonding to the block copolymer. The bonding is phenyl ester bond, which is stable under acidic condition and labile under mild alkaline condition. These results indicate that NK012 can release SN-38 under neutral condition even without the presence of a hydrolytic enzyme and is stable in 5% glucose solution. It is suggested that NK012 is stable before administration and starts to release SN-38, the active component, under physiologic conditions after administration.

Cellular sensitivity of non–small-cell lung cancer and colon cancer cells to SN-38, NK012, and CPT-11. The IC_{50} values of NK012 for the cell lines ranged from 0.009 μmol/L (SBC-3 cells) to 0.16 μmol/L (WiDR cells). The growth inhibitory effects of NK012 are 43- to 340-fold more potent than those of CPT-11, whereas the IC_{50} values of NK012 were 2.3- to 5.8-fold higher than those of SN-38. NK012 exhibited a higher cytotoxic effect against each cell line as compared with CPT-11 (43- to 340-fold sensitivity). On the other hand, the IC_{50} values of NK012 were a little higher than those of SN-38, similar to the cytotoxic feature also reported in a previous study about micellar drugs (ref. 23; Table 1).

Antitumor activity and pharmacokinetic analysis of NK012 and CPT-11 using HT-29–bearing nude mice (experiment 1). Potent activity was observed in mice treated with NK012 at doses of 15 and 30 mg/kg (Fig. 2*A*), although neither CPT-11 at a dose of 66.7 mg/kg/d nor NK012 at a dose of 7.5 mg/kg/d exerted any significant antitumor activity *in vivo*. Comparison of the relative tumor volume at day 21 revealed significant differences between 15 mg/kg/d NK012 and 66.7 mg/kg/d CPT-11 and between 30 mg/kg/d NK012 and 66.7 mg/kg/d CPT-11 ($P < 0.05$). Although treatment-related body weight loss was observed in mice treated with each drug, body weight recovered by day 21 (Fig. 2*B*). These results clearly show the significant *in vivo* activity of NK012 against HT-29.

After injection of CPT-11, the concentrations of CPT-11 and SN-38 for plasma declined rapidly with time in a log-linear fashion. On the other hand, NK012 (polymer-bound SN-38) exhibited slower clearance (Fig. 3*A*). The clearance of NK012 in the HT-29 tumor was significantly slower and the concentration of free SN-38 was maintained at >30 ng/g even at 168 hours after injection (Fig. 3*B*). The pharmacokinetic variables of each drug in the plasma and tumor are depicted in Table 2.

Tumor-to-plasma concentration ratios (Kp) of polymer-bound and free SN-38 increased during the observation period. The highest value of Kp was achieved at 168 hours after administration, 108 for polymer-bound and 11.0 for free SN-38 (Table 3). These results indicate that NK012 can remain in the tumor tissue for a longer period and release free SN-38.

Antitumor activity and the distribution of NK012 and CPT-11 in SBC-3/Neo or SBC-3/VEGF tumors (experiment 2). To determine whether the potent antitumor effect of NK012 is enhanced in the tumors with high vascularity, we used VEGF-secreting cells SBC-3/VEGF. There was no significant difference in the *in vitro* cytotoxic activity of each drug between SBC-3/Neo and SBC-3/VEGF (Fig. 4*A*). SBC-3/VEGF tumors are reddish by gross evaluation as compared with SBC-3/Neo tumors (Fig. 4*B*). Histologic and immunohistochemical (von Willebrand factor) examination revealed that prominent leakage of erythrocytes and high vascularity were observed in SBC-3/VEGF tumor xenografts. On the other hand, SBC-3/Neo tumors have less tumor vasculatures and more interstitial space as compared with SBC-3/VEGF tumors

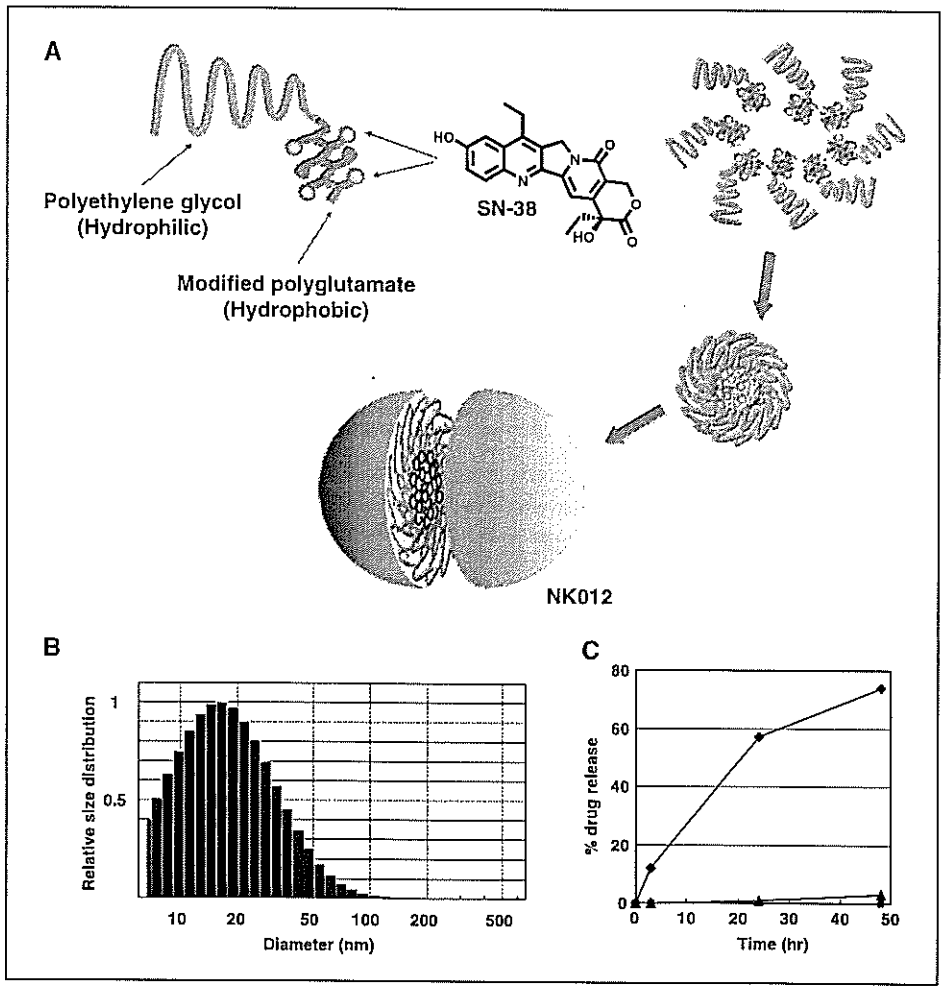

Figure 1. Preparation and characterization of NK012. *A*, schematic structure of NK012. A polymeric micelle carrier of NK012 consists of a block copolymer of PEG (molecular weight of ~12,000) and partially modified polyglutamate (~20 units). PEG (hydrophilic) is believed to be the outer shell and SN-38 was incorporated into the inner core of the micelle. *B*, size distribution of NK012 measured with the dynamic light scattering method. The *Y* axis shows relative particle size distribution. *C*, release of free SN-38 from the micelles in PBS [pH 7.3, 37°C (♦)] or 5% glucose solution [pH 4.6, 20°C (■), 37°C (▲)].

(Fig. 4*B*). Deviating from the ordinary experimental tumor model, tumors were allowed to grow until they became massive in size, ~1.5 cm (Fig. 4*C*), and then the treatment was initiated. NK012 at doses of 15 and 30 mg/kg showed potent antitumor activity against bulky SBC-3/Neo tumors (1,533.1 ± 1,204.7 mm^3) as compared with CPT-11 (Fig. 4*C*). Striking antitumor activity was observed in mice treated with NK012 (Fig. 4*C*) when we compared the antitumor activity of NK012 with that of CPT-11 using SBC-3/VEGF cells. SBC-3/VEGF bulky masses (1,620.7 ± 834.0 mm^3) disappeared in all mice, although relapse 3 months after treatment was noted in one mouse treated with NK012 20 mg/kg. On the other hand, SBC-3/VEGF were not eradicated and rapidly regrew after a partial response in mice treated with CPT-11. Approximately 10% body weight loss was observed in mice treated with 20 mg/kg NK012, but no significant difference was observed in comparison with mice treated with 30 mg/kg CPT-11.

We then examined the distribution of free SN-38 in the SBC-3/Neo and SBC-3/VEGF masses after administration of NK012 and CPT-11. In the case of CPT-11 administration, the concentrations at 1 and 6 hours after the administration were <100 ng/g both in the SBC-3/Neo and SBC-3/VEGF tumors and were almost negligible at 24 hours in both tumors (Fig. 5*A*). There was no significant difference in the concentration between the SBC-3/Neo and SBC-3/VEGF tumors. On the other hand, in the case of NK012 administration, free SN-38 was detectable in the tumors even at 72 hours after the administration. The concentrations of free SN-38 were higher in the SBC-3/VEGF tumors than those in the SBC-3/Neo tumors at any time point during the period of observation (significant at 1, 6, and 24 hours; $P < 0.05$; Fig. 5*A*).

Tissue distribution of SN-38 after administration of NK012 and CPT-11. We examined the concentration-time profile of free SN-38 in various tissues after i.v. administration of NK012 and

Table 1. *In vitro* growth inhibitory activity of SN-38, NK012, and CPT-11 in human lung and colorectal cancer cells (MTT assay)

Cell line	IC_{50} (μmol/L)		
	SN-38	NK012	CPT-11
WiDR	0.046 ± 0.008	0.16 ± 0.014	20.4 ± 1.6
SW480	0.025 ± 0.003	0.11 ± 0.028	31.9 ± 1.3
Lovo	0.0067 ± 0.0012	0.026 ± 0.003	7.24 ± 1.04
HT-29	0.016 ± 0.003	0.068 ± 0.007	23.1 ± 2.63
PC-14	0.044 ± 0.025	0.14 ± 0.021	5.96 ± 0.90
SBC-3	0.0016 ± 0.001	0.0093 ± 0.005	0.72 ± 0.22
A431	0.0081 ± 0.002	0.019 ± 0.007	5.6 ± 1.5

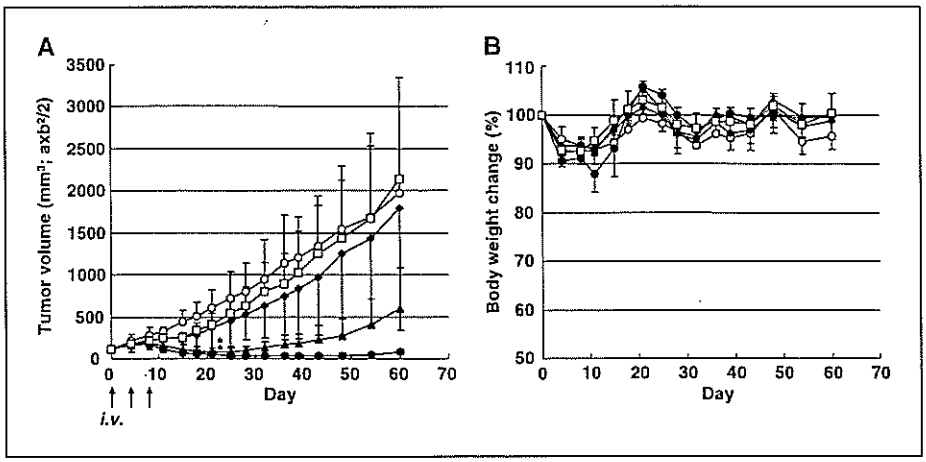

Figure 2. The effect of NK012 and CPT-11 against an HT-29 tumor xenograft. *A*, HT-29 tumor was inoculated s.c. into the flank of mice as described in Materials and Methods. CPT-11 at a dose of 66.7 mg/kg/d (□), NK012 at a dose of 7.5 mg/kg/d (♦), NK012 at a dose of 15 mg/kg/d (▲), or NK012 at a dose of 30 mg/kg/d (●) was administered i.v. on days 0, 4, and 8 (○, no treatment). Tumor volume in mice treated with CPT-11 or NK012. *Points*, mean; *bars*, SD. *, $P < 0.05$. *B*, treatment-related body weight loss occurred in mice treated with CPT-11 and NK012. *Points*, mean; *bars*, SD.

CPT-11. All organs measured exhibited the highest concentration of SN-38 at 1 hour after administration in mice given CPT-11 (Fig. 5*B*). On the other hand, mice given NK012 exhibited prolonged distribution in the liver and spleen (Fig. 5*B*). In a similar manner to other micellar drugs (19, 23), NK012 showed relatively higher accumulation in organs of the reticuloendothelial system. In the lung, kidney, and small intestine, the highest concentration of free SN-38 was achieved at 1 hour after injection of NK012 and the concentration was almost negligible at 24 hours. Although relatively high at 1 hour after administration of NK012 and CPT-11, the concentrations of free SN-38 in the small intestine rapidly decreased. Interestingly, there was no significant difference in the kinetic character of free SN-38 in the small intestine between mice treated with NK012 and CPT-11.

Discussion

The drug-incorporating polymeric micelle has characteristic pharmacokinetic features. These structures are too large to pass through normal vessel walls and evade renal excretion. The outer shell of the drug with PEG diminishes nonspecific capture by the reticuloendothelial system. Therefore, the drug can be expected to achieve a long half-life, which permits a large amount of the drug-incorporating micelles to reach the tumor site through the enhanced permeability and retention effect. The pharmacokinetic study revealed that the plasma AUC of polymer-bound SN-38 after administration of NK012 at a dose of 30 mg/kg to the HT-29-bearing mice was ~200-fold higher than that of CPT-11 at a dose of 66.7 mg/kg. A 14-fold higher AUC of the free SN-38 was achieved in mice given NK012 compared with mice given CPT-11. Prolonged circulation of NK012 in the blood might increase the accumulation of NK012 in a tumor tissue due to the enhanced permeability and retention effect. In fact, the tumor concentration of free SN-38 at 24 hours after administration of NK012 reached 90.4 ng/g and high concentrations were maintained up to 168 hours (53.1 ng/g for 48 hours, 42.6 ng/g for 72 hours, and 35.8 ng/g for 168 hours). This range of concentrations can exert sufficient antitumor activity against tumor cells. On the other hand, the concentration of CPT-11 was only 4.5 ng/g at 24 hours. These results indicate that the enhancement of tumor distribution closely contributes to the potent antitumor activity of NK012 *in vivo*.

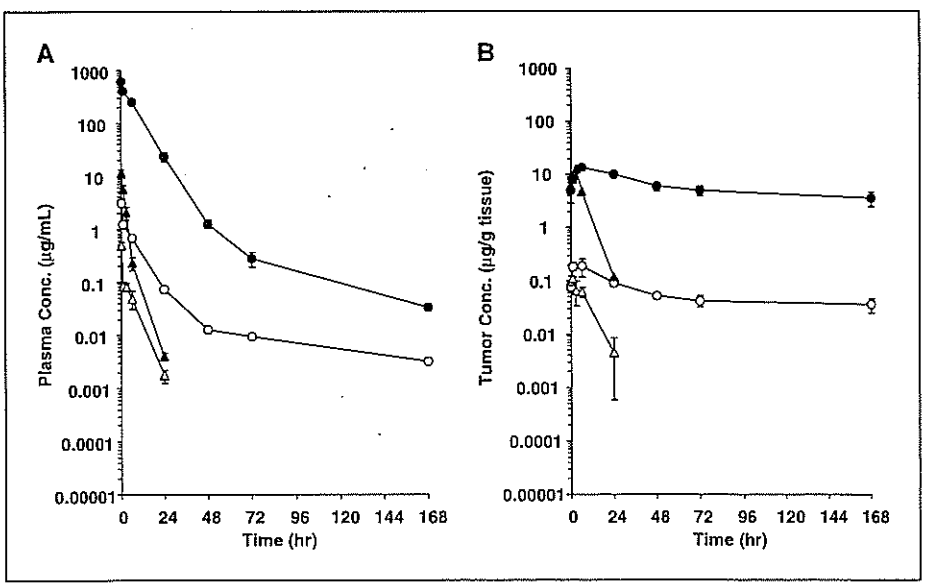

Figure 3. Plasma and tumor concentrations of respective analytes after an i.v. administration of CPT-11 (66.7 mg/kg) or NK012 (30 mg/kg) to HT-29-bearing nude mice. *A*, plasma. *B*, tumor. ●, polymer-bound SN-38; ○, free SN-38 (polymer-unbound SN-38); △, SN-38 converted from CPT-11; ▲, CPT-11.

Table 2. Pharmacokinetic variables of analytes in plasma and tumor after an i.v. administration of NK012 or CPT-11 to nude mice bearing human colon cancer HT-29 cells (NK012, 30 mg/kg; CPT-11, 66.7 mg/kg)

	Test article		C_{max} (μg/mL)	T_{max} (h)	$T_{1/2z}$ (h)	AUC_{last} (μg h/mL)	AUC_{inf} (μg h/mL)	CL_{tot} (mL/h/kg)	V_{ss} (mL/kg)	MRT_{last} (h)	$MRT_{inf.}$ (h)
Plasma	NK012	P-b SN-38*	—†	—	31.4	5,000	5,010	5.99	40.4	6.68	6.74
		P-u SN-38‡	3.10	0.0833	61.7	15.5	15.8	—	—	10.8	15.3
	CPT-11	CPT-11	—	—	3.08	22.1	22.2	3,010	5,420	1.78	1.80
		SN-38	0.488	0.0833	3.76	1.10	1.11	—	—	3.82	4.04
Tumor	NK012	P-b SN-38	13.8	6	—	1,010	—	—	—	62.8	—
		P-u SN-38	0.188	6	—	10.2	—	—	—	58.1	—
	CPT-11	CPT-11	12.6	3	3.36	99.7	100	—	—	4.41	4.55
		SN-38	0.108	1	4.75	1.07	1.10	—	—	5.20	5.92

NOTE: Three female nude mice were used for the analysis of biodistribution of SN-38 and CPT-11 in plasma and tissues. Data were expressed as means.
*Polymer-bound SN-38; SN-38 remaining bound to PEG-PGlu.
†Not determined.
‡Polymer-unbound SN-38; free SN-38 from PEG-PGlu.

Several preclinical studies on cytotoxic agent–incorporating polymeric micelles show their advantage as anticancer agents *in vivo* as compared with drugs of small molecular size (19, 22, 23). Because the advantage of passive targeting has been explained by the enhanced permeability and retention theory, it is essential to elucidate the correlation between the effectiveness of micellar drugs and tumor hypervascularity and hyperpermeability. We hypothesized that a polymeric micelle–based drug carrier could increase its accumulation in the tumor site and could thus enhance the therapeutic efficacy in tumors with high vascularity. To ascertain the hypothesis, we used SBC-3/VEGF. We adopted a bulky tumor model for our *in vivo* experiment to clarify the difference in activity against SBC-3/Neo and SBC-3/VEGF tumors. Histologic examination of SBC-3/VEGF showed hypervascularity and prominent leakage of erythrocytes. On the other hand, SBC-3/Neo showed hypovascularity. Our *in vivo* experiment showed that NK012 obviously enhanced its antitumor activity in SBC-3/VEGF-inplanted mice and eradicated bulky masses. It was thought that the sensitivity of cells to NK012 might not change *in vivo* because the *in vitro* sensitivity of NK012 was almost equivalent between SBC-3/Neo and SBC-3/VEGF cells. When we compared the distribution of NK012 (free SN-38) in the tumor sites, significantly enhanced accumulation was observed in the SBC-3/VEGF tumors. This strongly suggested that the drug distribution throughout the tumor site was enhanced by the hypervascularity and hyperpermeability induced by VEGF, and, subsequently, higher antitumor activity was achieved. High vascular density and enhanced vascular permeability might also be favorable for drug delivery of low molecular weight drugs. However, the SN-38 concentration was not significantly high in SBC-3/VEGF tumors after the administration of CPT-11, and tumors exhibited rapid regrowth after the treatment. We assume that such conventional low molecular size anticancer agents almost disappear from the bloodstream without being subjected to the enhanced permeability and retention effect before they can reach the target organs (solid tumor). The fact of correlation between the blood vessel density in

Table 3. Tumor-to-plasma concentration ratio (Kp) of analytes after an i.v. administration of NK012 (30 mg/kg) to nude mice bearing human colon cancer HT-29 cells

Test article	Analyte		Time after administration (h)						
			0.0833	1	6	24	48	72	168
NK012	P-b SN-38*	Plasma (μg/mL)	612	410	254	23.3	1.25	0.278	0.0333
		Tumor (μg/g)	4.99	8.00	13.8	9.95	5.90	5.03	3.58
		Kp† (mL/g)	0.00815	0.0195	0.0543	0.427	4.72	18.1	108
	P-u SN-38‡	Plasma (μg/mL)	3.10	1.24	0.673	0.0717	0.0127	0.00925	0.00325
		Tumor (μg/g)	0.0763	0.187	0.188	0.0904	0.0531	0.0426	0.0358
		Kp (mL/g)	0.0246	0.151	0.279	1.26	4.18	4.61	11.0

NOTE: Data were expressed as means of three mice.
*Polymer-bound SN-38; SN-38 remaining bound to PEG-PGlu.
†Kp values were calculated on the mean concentrations of three mice.
‡Polymer-unbound SN-38; free SN-38 from PEG-PGlu.

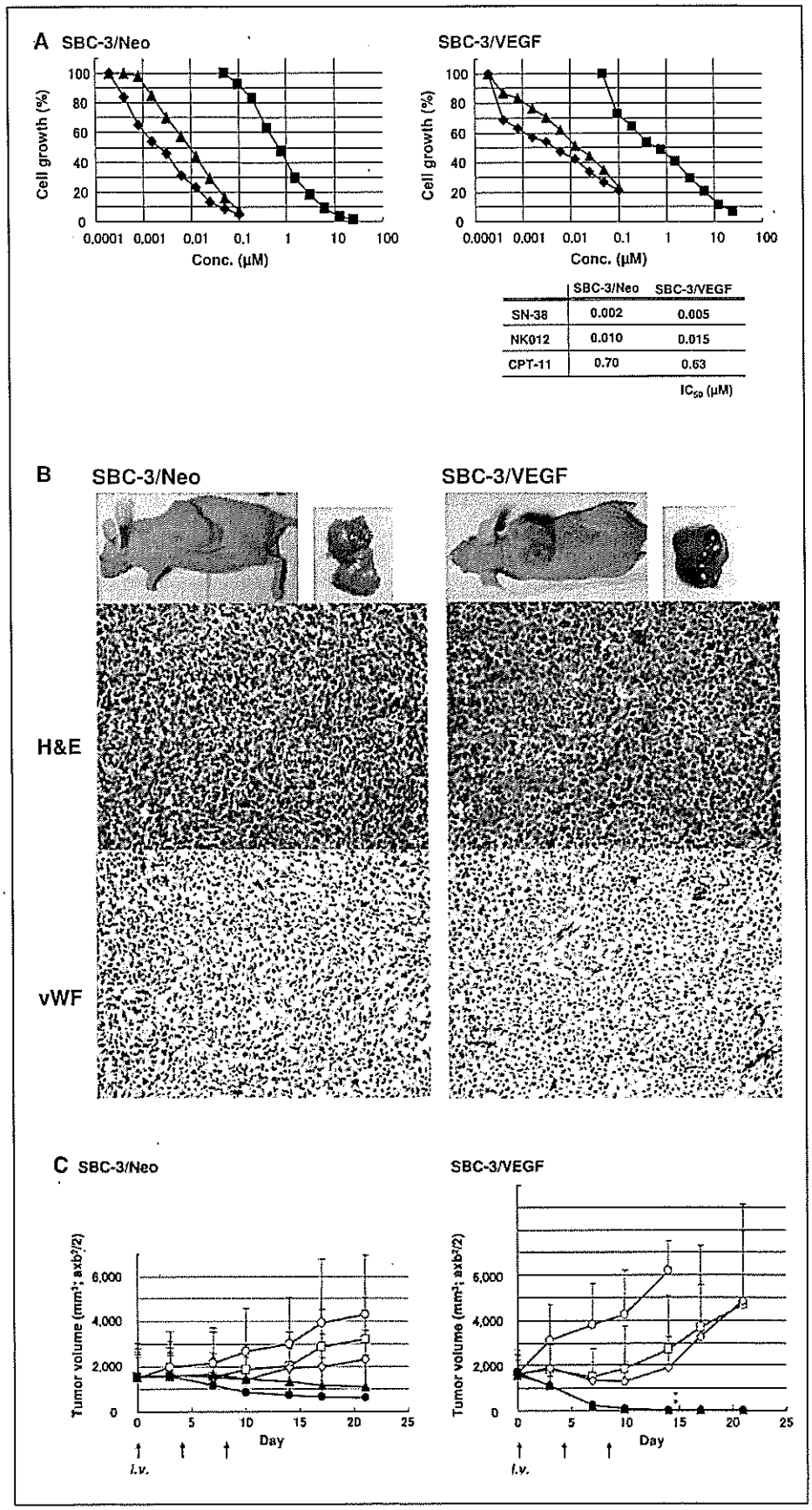

Figure 4. Growth inhibitory effect of NK012, SN-38, and CPT-11 on SBC-3/Neo and SBC-3/VEGF cells. *A*, in *in vitro* experiment, the cells were exposed to the indicated concentrations of each drug for 72 hours. The growth inhibition curves and IC_{50} values for NK012 (▲), SN-38 (◆), and CPT-11 (■) are shown. *B*, representative photographs of massive tumors developed from SBC-3/Neo and SBC-3/VEGF at the time just before treatment initiation. Histologic (H&E, ×20) and immunohistochemical (von Willebrand factor, ×20) examinations for each tumor are shown. *C*, i.v. administration of NK012 or CPT-11 was started when the mean tumor volumes of groups reached a massive size of 1,500 mm^3. The mice were divided into test groups (○, control; □, CPT-11 15 mg/kg/d; ◇, CPT-11 30 mg/kg/d; ▲, NK012 10 mg/kg/d; ●, NK012 20 mg/kg/d). NK012 or CPT-11 was administered i.v. on days 0, 4, and 8. Each group consisted of four mice. *, $P < 0.05$.

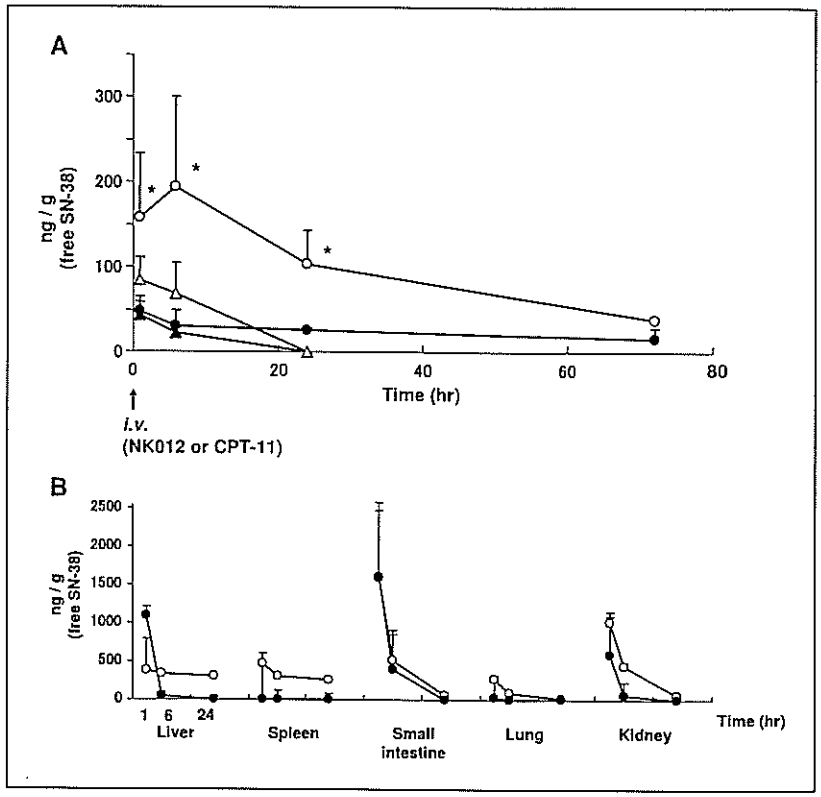

Figure 5. Tissue and tumor distribution of free SN-38 after administration of NK012 and CPT-11. *A*, time profile of free SN-38 concentration in SBC-3/Neo (●, NK012 20 mg/kg/d; ▲, CPT-11 30 mg/kg/d) and SBC-3/VEGF (○,NK012 20 mg/kg/d; △, CPT-11 30 mg/kg/d). NK012 on days 0 and 4 (96 hours) or CPT-11 on day 0 was administered. *, $P < 0.05$. *B*, tissue distribution of free SN-38 after single injection of NK012 at 30 mg/kg (○) and CPT-11 at 40 mg/kg (●).

the tumor mass and poor prognosis for survival in people with various types of cancers (25–28) supports the idea that low molecular weight drugs are not so effective in the treatment of solid tumors, which are rich in blood vessels.

Jain (35) reported that the convective passage of large drug molecules into the core of solid tumors could be impeded by abnormally high interstitial pressures in solid tumors. However, he also considered that low molecular weight anticancer agents might be harmful to normal organs because they can leak out of normal blood vessels freely; he finally concluded that one useful strategy for evading the barriers to drug dispersion would be to inject patients with drug carriers, such as liposome, filled with low molecular weight drugs. NK012 has the potential to allow the effective sustained release of SN-38 inside a tumor following the accumulation of NK012 into tumor tissue. As a matter of fact, substantial amount of SN-38 is expected to be released from the polymeric micelle. Consequently, released SN-38 becomes distributed throughout the tumor tissue and internalizes into cancer cells to kill them.

In recent years, the novel liposome-based formulation of SN-38 (LE-SN38) has been developed (36). LE-SN38 shows promising antitumor activity against various cancer cell lines (37, 38) and a clinical trial to assess its efficacy is now under way (39). The release of SN-38 from LE-SN38 is very slow as compared with NK012, ~1.9% of the drug being released from LE-SN38 in PBS buffer over 120 hours (36). The size of LE-N38 ranges from 150 to 200 nm. On the other hand, the particle size of NK012 is ~20 nm. Interestingly, Unezaki et al. (40) reported that fluorescence-labeled PEG liposomes were densely located outside the tumor vessels and stayed around the vessel walls for 2 days after i.v. injection. These data suggest that the PEG liposome is too large to move freely in the tumor interstitium and too stable to be released easily. The difference in size distribution and the character of the drug release between NK012 and LE-SN38 might influence their clinical effectiveness in the treatment of solid tumors.

One of the major toxicities associated with CPT-11 administration is severe diarrhea. Although the mechanism of the diarrhea has not yet been elucidated, one possible explanation is structural and functional injuries to the gastrointestinal tract owing to the mitotic inhibitory activity of SN-38 and CPT-11. It was reported that the number of episodes of diarrhea had a better correlation with the plasma AUC of SN-38 than with CPT-11 (41). In the present study, no difference in SN-38 accumulations in the small intestine was seen when equimolar NK012 (20 mg/kg) and CPT-11 (30 mg/kg) were administered. We also reported, using a rat mammary tumor model, that NK012 showed significant antitumor effect with diminishing incidence of diarrhea as compared with CPT-11 (42). These results suggest that diarrhea, one of the dose-limiting toxicities of CPT-11, is not augmented by the administration of NK012.

In conclusion, the present data suggest that NK012 possesses a treatment advantage over CPT-11, especially in hypervascular tumors such as renal cell carcinomas, medulloblastomas, and hepatocellular carcinomas. We have now started a phase I clinical trial for NK012 in patients with advanced solid tumors.

Acknowledgments

Received 5/3/2006; revised 7/20/2006; accepted 8/21/2006.

The costs of publication of this article were defrayed in part by the payment of page charges. This article must therefore be hereby marked *advertisement* in accordance with 18 U.S.C. Section 1734 solely to indicate this fact.

References

1. Li LH, Fraser TJ, Olin EJ, Bhuyan BK. Action of camptothecin on mammalian cells in culture. Cancer Res 1972;32:2643–50.
2. Gallo RC, Whang-Peng J, Adamson RH. Studies on the antitumor activity, mechanism of action, and cell cycle effects of camptothecin. Natl Cancer Inst 1971; 46:789–95.
3. Gottlieb JA, Guarino AM, Call JB, Oliverio VT, Block JB. Preliminary pharmacologic and clinical evaluation of camptothecin sodium (NSC-100880). Cancer Chemother Rep 1970;54:461–70.
4. Muggia FM, Creaven PJ, Hansen HH, Cohen MH, Selawry OS. Phase I clinical trial of weekly and daily treatment with camptothecin (NSC-100880): correlation with preclinical studies. Cancer Chemother Rep 1972;56: 515–21.
5. Cunningham D, Pyrhonen S, James RD, et al. Randomised trial of irinotecan plus supportive care versus supportive care alone after fluorouracil failure for patients with metastatic colorectal cancer. Lancet 1998; 352:1413–8.
6. Saltz LB, Cox JV, Blanke C, et al. Irinotecan plus fluorouracil and leucovorin for metastatic colorectal cancer. Irinotecan Study Group. N Engl J Med 2000;343: 905–14.
7. Noda K, Nishiwaki Y, Kawahara M, et al. Irinotecan plus cisplatin compared with etoposide plus cisplatin for extensive small-cell lung cancer. N Engl J Med 2002; 346:85–91.
8. Negoro S, Masuda N, Takada Y, et al. CPT-11 Lung Cancer Study Group West. Randomised phase III trial of irinotecan combined with cisplatin for advanced non-small-cell lung cancer. Br J Cancer 2003; 88:335–41.
9. Bodurka DC, Levenback C, Wolf JK, et al. Phase II trial of irinotecan in patients with metastatic epithelial ovarian cancer or peritoneal cancer. J Clin Oncol 2003; 21:291–7.
10. Takimoto CH, Arbuck SG. Topoisomerase I targeting agents: the camptothecins. In: Chabner BA, Lango DL, editors. Cancer chemotherapy and biotherapy: principal and practice. 3rd ed. Philadelphia (PA): Lippincott Williams & Wilkins; 2001. p. 579–646.
11. Slatter JG, Schaaf LJ, Sams JP, et al. Pharmacokinetics, metabolism, and excretion of irinotecan (CPT-11) following I.V. infusion of [(14)C]CPT-11 in cancer patients. Drug Metab Dispos 2000;28:423–33.
12. Rothenberg ML, Kuhn JG, Burris HA III, et al. Phase I and pharmacokinetic trial of weekly CPT-11. J Clin Oncol 1993;11:2194–204.
13. Guichard S, Terret C, Hennebelle I, et al. CPT-11 converting carboxylesterase and topoisomerase activities in tumour and normal colon and liver tissues. Br J Cancer 1999;80:364–70.
14. Matsumura Y, Maeda H. A new concept for macromolecular therapeutics in cancer chemotherapy: mechanism of tumoritropic accumulation of proteins and the antitumor agent smancs. Cancer Res 1986;46: 6387–92.
15. Dvorak HF, Nagy JA, Dvorak JT, Dvorak AM. Identification and characterization of the blood vessels of solid tumors that are leaky to circulating macromolecules. Am J Pathol 1988;133:95–109.
16. Maeda H, Matsumura Y. Tumoritropic and lymphotropic principles of macromolecular drugs. Crit Rev Ther Drug Carrier Syst 1989;6:193–210.
17. Matsumura Y, Maruo K, Kimura M, Yamamoto T, Konno T, Maeda H. Kinin-generating cascade in advanced cancer patients and *in vitro* study. Jpn J Cancer Res 1991;82:732–41.
18. Yokoyama M, Miyauchi M, Yamada N, et al. Characterization and anticancer activity of the micelle-forming polymeric anticancer drug Adriamycin-conjugated poly(ethylene glycol)-poly(aspartic acid) block copolymer. Cancer Res 1990;50:1693–700.
19. Yokoyama M, Okano T, Sakurai Y, Ekimoto H, Shibazaki C, Kataoka K. Toxicity and antitumor activity against solid tumors of micelle-forming polymeric anticancer drug and its extremely long circulation in blood. Cancer Res 1991;51:3229–36.
20. Kataoka K, Harada A, Nagasaki Y. Block copolymer micelles for drug delivery: design, characterization and biological significance. Adv Drug Deliv Rev 2001;47: 113–31.
21. Matsumura Y, Hamaguchi T, Ura T, et al. Phase I clinical trial and pharmacokinetic evaluation of NK911, a micelle-encapsulated doxorubicin. Br J Cancer 2004;91: 1775–81.
22. Hamaguchi T, Matsumura Y, Suzuki M, et al. NK105, a paclitaxel-incorporating micellar nanoparticle formulation, can extend *in vivo* antitumour activity and reduce the neurotoxicity of paclitaxel. Br J Cancer 2005; 92:1240–6.
23. Uchino H, Matsumura Y, Negishi T, et al. Cisplatin-incorporating polymeric micelles (NC-6004) can reduce nephrotoxicity and neurotoxicity of cisplatin in rats. Br J Cancer 2005;93:678–87.
24. Folkman J. Anti-angiogenesis: new concept for therapy of solid tumors. Ann Surg 1972;175:409–16.
25. Gasparini G, Harris AL. Clinical importance of the determination of tumor angiogenesis in breast carcinoma: much more than a new prognostic tool. J Clin Oncol 1995;13:765–82.
26. Dickinson AJ, Fox SB, Persad RA, Hollyer J, Sibley GN, Harris AL. Quantification of angiogenesis as an independent predictor of prognosis in invasive bladder carcinomas. Br J Urol 1994;74:762–6.
27. Takahashi Y, Kitadai Y, Bucana CD, Cleary KR, Ellis LM. Expression of vascular endothelial growth factor and its receptor, KDR, correlates with vascularity, metastasis, and proliferation of human colon cancer. Cancer Res 1995;55:3964–8.
28. Williams JK, Carlson GW, Cohen C, Derose PB, Hunter S, Jurkiewicz MJ. Tumor angiogenesis as a prognostic factor in oral cavity tumors. Am J Surg 1994; 168:373–80.
29. Natsume T, Watanabe J, Koh Y, et al. Antitumor activity of TZT-1027 (Soblidotin) against vascular endothelial growth factor-secreting human lung cancer *in vivo*. Cancer Sci 2003;94:826–33.
30. Stacker SA, Caesar C, Baldwin ME, et al. VEGF-D promotes the metastatic spread of tumor cells via the lymphatics. Nat Med 2001;7:186–91.
31. Amoroso A, Del Porto F, Di Monaco C, Manfredini P, Afeltra A. Vascular endothelial growth factor: a key mediator of neoangiogenesis. A review. Eur Rev Med Pharmacol Sci 1997;1:17–25.
32. Cabral H, Nishiyama N, Okazaki S, Koyama H, Kataoka K. Preparation and biological properties of dichloro(1,2-diaminocyclohexane)platinum(II) (DACHPt)-loaded polymeric micelles. J Controlled Res 2005;101: 223–32.
33. Nishiyama N, Yokoyama M, Aoyagi T, Okano T, Sakurai Y, Kataoka K. Preparation and characterization of self-assembled polymer-metal complex micelle from *cis*-dichlorodiammineplatinum(II) and poly(ethylene glycol)-poly(α,β-aspartic acid) block copolymer in an aqueous medium. Langmuir 1999;15:377–83.
34. Kawato Y, Furuta T, Aonuma M, Yasuoka M, Yokokura T, Matsumoto K. Antitumor activity of a camptothecin derivative, CPT-11, against human tumor xenografts in nude mice. Cancer Chemother Pharmacol 1991;28:192–8.
35. Jain RK. Barriers to drug delivery in solid tumors. Sci Am 1994;271:58–65.
36. Zhang JA, Xuan T, Parmar M, et al. Development and characterization of a novel liposome-based formulation of SN-38. Int J Pharm 2004;270:93–107.
37. Lei S, Chien PY, Sheikh S, Zhang A, Ali S, Ahmad I. Enhanced therapeutic efficacy of a novel liposome-based formulation of SN-38 against human tumor models in SCID mice. Anticancer Drugs 2004;15:773–8.
38. Pal A, Khan S, Wang YF, et al. Preclinical safety, pharmacokinetics and antitumor efficacy profile of liposome-entrapped SN-38 formulation. Anticancer Res 2005;25:331–41.
39. Kraut EH, Fishman MN, LoRusso PM, et al. Final result of a phase I study of liposome encapsulated SN-38 (LE-SN38): safety, pharmacogenomics, pharmacokinetics, and tumor response [abstract 2017]. Proc Am Soc Clin Oncol 2005;23:139s.
40. Unezaki S, Maruyama K, Hosoda JI, et al. Direct measurement of the extravasation of polyethyleneglycol-coated liposomes into solid tumor tissue by *in vivo* fluorescence microscopy. Int J Pharmaceut 1996;144: 11–7.
41. Sasaki Y, Yoshida Y, Sudoh K, et al. Pharmacological correlation between total drug concentration and lactones of CPT-11 and SN-38 in patients treated with CPT-11. Jpn J Cancer Res 1995;86:111–6.
42. Onda T, Nakamura I, Seno C, et al. Superior antitumor activity of NK012, 7-ethyl-10-hydroxycamptothecin-incorporating micellar nanoparticle, to irrinotecan [abstract 3062]. Proc Am Assoc Cancer Res 2006;47: 720s.

Lung Cancer (2006) 53, 13–21

available at www.sciencedirect.com

SCIENCE DIRECT

journal homepage: www.elsevier.com/locate/lungcan

LUNG CANCER

Effects of different combinations of gefitinib and irinotecan in lung cancer cell lines expressing wild or deletional EGFR

Tatsu Shimoyama[a,b], Fumiaki Koizumi[a], Hisao Fukumoto[a], Katsuyuki Kiura[b], Mitsune Tanimoto[b], Nagahiro Saijo[a], Kazuto Nishio[a,*]

[a] *Shien-Lab and Medical Oncology, National Cancer Center Hospital, Pharmacology Division, National Cancer Center Research Institute, Tsukiji 5-1-1, Chuo-ku, Tokyo 104-0045, Japan*
[b] *Department of Medicine II, Okayama University Medical School, 2-5-1 Shikata-cho, Okayama 700-8558, Japan*

Received 8 November 2005; accepted 1 March 2006

KEYWORDS
Gefitinib;
CPT-11;
SN-38;
EGFR;
Combination;
Lung cancer

Summary EGFR mutations are a major determinant of lung tumor response to gefitinib, an EGFR-specific tyrosine kinase inhibitor. Obtaining a response from lung tumors expressing wild-type EGFR is a major obstacle. The combination of gefitinib and cytotoxic drugs is one strategy against lung cancers expressing wild-type EGFR. The DNA topoisomerase inhibitor irinotecan sulfate (CPT-11) is active against lung cancer. We examined the sensitivity of lung cancers expressing wild- or mutant-type EGFR to the combination of gefitinib and CPT-11. The in vitro effect of gefitinib and SN-38 (the active metabolite of CPT-11) was examined in seven lung cancer cell lines using the dye formation assay with a combination index. When administered concurrently, gefitinib and SN-38 had a synergistic effect in five of the seven cell lines expressing wild-type EGFR, whereas the combination was antagonistic in PC-9 cells and a PC-9 subline resistant to gefitinib and expressing deletional mutant EGFR (PC-9/ZD). When administered sequentially, treatment with SN-38 followed by gefitinib had remarkable synergistic effects in the PC-9 and PC-9/ZD cells. In an in vivo tumor-bearing model, this combination had a schedule-dependent synergistic effect in the PC-9 and PC-9/ZD cells. An immunohistochemical analysis of the tumors in mice treated with CPT-11 and gefitinib demonstrated that the number of Ki-67 positive tumor cells induced by CPT-11 treatment was decreased when CPT-11 was administered in combination with gefitinib. In conclusion, the sequential combination of CPT-11 and gefitinib is considered to be active against lung cancer.

1. Introduction

Lung cancer is one of the leading causes of cancer-related death, despite the use of conventional chemotherapy regi-

* Corresponding author at: Tel.: +81 3 3542 2511; fax: +81 3 3547 5185.
E-mail address: knishio@gan2.res.ncc.go.jp (K. Nishio).

0169-5002/$ – see front matter © 2006 Elsevier Ireland Ltd. All rights reserved.
doi:10.1016/j.lungcan.2006.03.014

mens. The epidermal growth factor receptor (EGFR) is frequently expressed in non-small cell lung cancer (NSCLC) and is correlated with a poor prognosis. Gefitinib ('Iressa') is an orally active, selective EGFR-tyrosine kinase inhibitor that blocks signal transduction pathways. Its clinical efficacy has been show in refractory NCSLC patients, but the survival benefit of this agent remains unclear. EGFR mutations have been identified in NSCLC, and lung cancers carrying the EGFR mutation have been reported to be hyperresponsive to gefitinib [1,2]. Mutant EGFR is a major determinant of lung tumor response to gefitinib, but the hyperresponsiveness of tumors expressing mutant EGFR has been observed in a small population. Now, obtaining a clinical benefit in lung tumors expressing wild-ype EGFR is a major obstacle. The combination of gefitinib and cytotoxic drugs is one strategy against lung cancers expressing wild-type EGFR. The DNA topoisomerase I inhibitor irinotecan (CPT-11) is a key drug in the treatment of patients with lung cancer and has been shown to prolong survival. SN-38 is the active metabolite of CPT-11 in vitro. The objective of this study was to determine the potential therapeutic utility of gefitinib when combined with CPT-11 therapy to lung cancer cell according to the treatment schedule and EGFR status.

Acquired resistance to gefitinib is also of clinical interest. Recently, Kobayashi et al. [3] reported that an EGFR mutation was related to the development of acquired resistance to gefitinib. We have established subclone PC-9/ZD cells that are resistant to gefitinib [4]. Our results suggested that another mechanism of resistance was active in PC-9/ZD cells. The effect of the combination of gefitinib and SN-38 in these PC-9/ZD cells was also examined.

2. Materials and methods

2.1. Drugs and chemicals

Gefitinib (*N*-(3-chloro-4-fluorophenyl)-7-methoxy-6-[3-(morpholin-4-yl)propoxy]quinazolin-4-amine) was provided by AstraZeneca (Cheshire, UK). Gefitinib was dissolved in dimethyl sulfoxide (DMSO) for the in vitro study. CPT-11 and SN-38 were obtained from Yakult Honsha (Tokyo, Japan) and were dissolved in dimethyl sulfoxide (DMSO) for both of the in vitro studies.

2.2. Cells and cultures

Human NSCLC cell lines PC-9, PC-7, and PC-14 derived from untreated patients with pulmonary adenocarcinoma were provided by Professor Y. Hayata, Tokyo Medical College. A small cell lung cancer cell line, H69, was established at the National Cancer Institute (Bethesda, MD, USA). The gefitinib-resistant subline, PC-9/ZD, was established from intrinsic hypersensitive cell PC-9 [5] in our laboratory [4]. A small cell lung cancer cell line, SBC-3, and an adenocarcinoma cell line, A549, were obtained from the Japanese Cancer Research Resources Bank (Tokyo, Japan). All cell lines were maintained in RPMI1640 (Nikken Bio Med. Lab., Kyoto, Japan) supplemented with 10% heat-inactivated fetal calf serum, 100 μg/ml streptomycin, and 100 units/ml penicillin in an incubator at 37 °C and 100% humidity in 5% CO_2 and air, as described previously [6].

2.3. RT-PCR

Specific primers designed for EGFR CDS were used to detect the EGFR mRNA, as described elsewhere [1]. Sixteen first-strand cDNAs were synthesized from the cells' RNA using an RNA PCR Kit (TaKaRa Biomedicals, Ohtsu, Japan). After the reverse transcription of 1 μg of total RNA with Oligo(dT)-M4 adaptor primer, the whole mixture was used for PCR with two oligonucleotide primers (5'-AATGTGAGCAGAGGCAGGGA-3' and 5'-GGCTTGGTTTGGAGCTTCTC-3). PCR was performed with an initial denaturation at 94 °C for 2 min and 25 cycles of amplification (denaturation at 94 °C for 30 s, annealing at 55 °C for 60 s, and extension at 72 °C for 105 s).

2.4. Western blot analysis

The cultured cells were washed twice with ice-cold phosphate buffered saline (PBS), lysate in EBC buffer (50 mM Tris–HCl, pH 8.0; 120 mM NaCl; 0.5% Nonidet P-40; 100 mM NaF; 200 mM Na orthovanadate; and 10 mg/ml each of leupeptin, aprotinin and phenylmethylsulfonyl fluoride). The lysate was cleared by centrifugation at 20,000 × *g* for 5 min, and the protein concentration of the supernatant was measured using a BCA protein assay (Pierce, Rockford, IL, USA). For immunoblotting, 20 μg samples of protein were electrophoretically separated on a 7.5% SDS-polyacrylamide gel and transferred to a polyvinylidene difluoride (PVDF) membrane (Millipore, Bedford, MA, USA). The membrane was then probed with rabbit polyclonal antibodies against EGFR, HER2/neu, Her3 and Her4 (Santa Cruz Biotech, Santa Cruz, CA, USA) and phospho-EGFR specific for Tyr 845, Tyr 1045, and Tyr 1068 (numbers 2231, 2235 and 2234; Cell Signaling, Beverly, MA, USA).

2.5. Growth-inhibition assay

We used the tetrazolium dye (3,(4,5-dimethyl-2-thiazolyl)-2,5-diphenyl-2H-tetrazolium bromide, MTT) assay to evaluate the cytotoxicity of various drug concentrations. After incubation for 72 h at 37 °C, 20 μl of MTT solution (5 mg/ml in PBS) was added to each well; the plates were then incubated for a further 4 h at 37 °C. After centrifuging the plates at 200 × *g* for 5 min, the medium was aspirated from each well and 180 μl of dimethylsulfoxide was added to each well to dissolve the formazan. Optical density was measured at 562 and 630 nm using a Delta Soft ELISA analysis program interfaced with a Bio-Tek Microplate Reader (EL-340; Bio-Metallics, Princeton, NJ, USA). Each experiment was performed in six replicate wells for each drug concentration and was independently performed three or four times. The IC_{50} value was defined as the concentration needed for a 50% reduction in the absorbance, as calculated based on the survival curves. Percent survival was calculated as follows:

$$\frac{\text{Mean absorbance of six replicate wells containing drugs} - \text{mean absorbance of six replicate background wells}}{\text{mean absorbance of six replicate drug-free wells} - \text{mean absorbance of six replicate background wells}} \times 100.$$

2.6. Combined effect of gefitinib and SN-38 in vitro

After 24 h of incubation, gefitinib and SN-38 were added to each cell line according to one of the two combination schedules. For the concurrent schedule, gefitinib and SN-38 were added concurrently and were then incubated under the same conditions for 72 h. For the sequential schedule, gefitinib or SN-38 were added sequentially and were then incubated under the same conditions for 72 h. The combined effect of gefitinib and SN-38 on lung cancer cell growth was evaluated using a combination index (CI) [7]. The CI was produced using CalcuSym software (Biosoft, NY, USA). For any given drug combination, the CI represents the degree of synergy, additivity, or antagonism. CI was expressed in terms of fraction-affected (F_a) values, which represents the percentage of cells killed or inhibited by the drug. Using mutually exclusive ($\alpha = 0$) or mutually non-exclusive ($\alpha = 1$) isobologram equations, the F_a/CI plots for each cell line were constructed by computer analysis of the data generated from the median effect analysis. The CI values were interpreted as follows: <1.0 = synergism; 1.0 = additive; >1.0 = antagonism.

2.7. In vivo growth-inhibition assay

Experiments were performed in accordance with the United Kingdom Coordinating Committee on Cancer Research Guidelines for the welfare of animals with experimental neoplasia (second edition). Fig. 2A shows the treatment schedule. For the in vivo experiments, the combined therapeutic effect of orally or intraperitoneally administered gefitinib and intravenously injected CPT-11 was evaluated according to a predetermined schedule. The dose of each drug was set based on the results of a preliminary experiment involving the administration of each drug alone. Ten days before administration, PC-9 and PC-9/ZD cells were injected subcutaneously into the backs of the mice. Six mice per group were injected with tumor cells. Tumor-bearing mice were given either gefitinib (40 mg/kg/day, p.o.) on days 2–6, CPT-11 (50 mg/kg/day, i.v.) on day 1, both, or a placebo (5%(w/v) glucose solution). Alternatively, tumor-bearing mice were given gefitinib on days 2–6 and CPT-1 on days 2. The diameters of the tumors were measured using calipers on days 1, 5, 8, 12, 15 and 20 to evaluate the effects of treatment, and tumor volume was determined using the following equation: tumor volume $ab^2/2$ (mm^3) (where a is the largest diameter of the tumor and b is the shortest diameter). Day 20 denotes the day on which the effects of the drugs were estimated, and day "0" denotes the first day of treatment. All mice were sacrificed on day 20 after their tumors had been measured.

2.8. Immunohistochemistry

The tumors were harvested from the mice at the time of sacrifice. For hematoxylin-eosin (HE) and anti-CD31 and Ki-67 staining, the resected tumors were fixed in zinc-buffered formalin (Shandon Lipshaw, Pittsburgh, PA) overnight at 4 °C. After paraffin embedding and sectioning at 6 μm, formalin-fixed sections were stained with Mayer's H&E (Richard Allen, Kalamazoo, MI, USA). For anti-Ki-67 and anti-CD31 immunohistochemistry, the slides were heated in a water bath at 95–99 °C in Target Retrieval Solution (DAKO, Carpinteria, CA, USA) for 20 min, followed by a 20-min cool-down period at room temperature. After heat retrieval, the sections were rinsed well in PBS and stained with rabbit antihuman Ki-67 antigen (DAKO N-series, ready to use) or rat antimouse CD-31 antibody (BD PharMingen, Tokyo, Japan) according to the manufacturer's instructions and then were lightly counterstained with Mayer's hematoxylin. The sections were finally stained with an in situ Death Detection POD Kit (Roche Diagnostic GmbH, Mannheim, Germany), according to the manufacturer's instructions.

TUNEL staining was performed using the Apoptosis Detection System, Fluorescein (Promega, Madison, WI, USA). Briefly, 6-μm cryostat sections were fixed in 4% paraformaldehyde for 10 min at room temperature and rinsed in PBS with 0.1% Triton X-100. The sections were then incubated in Equilibration Buffer for 5 min at room temperature followed by incubation in TUNEL Mix, prepared according to the manufacturer's instructions, for 1 h at 37 °C. After successive washes in PBS, the sections were coverslipped using an antifade reagent.

Microvessel density was determined by calculating the proportion of CD31-positive cells. The Proliferation Index was determined by Ki-67 immunostaining and calculating the population of Ki-67-positive cells in five fields at 200×. The Apoptosis Index, determined by TUNEL staining, was calculated from the population of TUNEL-positive cells in five fields at 200×. The apoptosis:proliferation ratio equals the apoptosis index/proliferation index × 100. At least 1000 tumor cell nuclei from the most evenly and distinctly labeled areas were examined in each examination.

At least 1000 cancer cells were counted and scored per slide. Both the percentage of specifically stained cells and the intensity of immunostaining were recorded. Blood vessels were detected with an anti-von Willebrand factor (vWF) antibody (Chemicon). Microvessel density was determined by calculating the proportion of vWF-positive cells.

3. Results

3.1. Expression of Her-receptors and cellular sensitivity to gefitinib or SN-38 in lung cancer cell lines

The expression levels of EGFR in seven lung cancer cell lines were examined using RT-PCR with a primer set for exon 20 in EGFR. PC-14, SBC-3, H69, PC-7, and A549 cells showed a 570-bp-long PCR amplified product exhibiting wild-type EGFR mRNA (data not shown). On the other hand, a smaller PCR product was also detected in the PC-9 and PC-9/ZD cells, and this band was confirmed to be an in-frame 15-base deletion of exon 20 (E746_A750del).

We examined the protein levels of EGFR, Her2, Her3, and Her4 in the lung cell lines using immunoblotting. The quantitative data obtained by densitometorical analysis is summarized in Table 1. The protein levels of EGFR, Her2, and Her3 in the PC-9 cells were one- to four-fold higher than those in the other cell lines (PC-7, H69, PC-14, A549, and SBC-3).

Table 1 Comparison of Her family protein levels and gefitinib- and SN-38-induced growth inhibition

Cell lines	Relative expression[a]				Growth inhibition[b], $IC_{50} \pm$S.D.	
	EGFR	Her2	Her3	Her4	Gefitinib (μM)	SN-38 (nM)
PC-9	2.8[c]	3.2	3.7	ND	0.047 ± 0.061	8.09 ± 1.9
PC-9/ZD	1.6[c]	2.6	3.8	ND	7.7 ± 0.5	38.9 ± 7.0
PC-14	1.5	2.8	1.1	ND	17.1 ± 0.8	42.1 ± 2.6
SBC-3	2.4	2.6	1.0	ND	19.9 ± 5.4	1.07 ± 0.1
A549	2.3	2.3	1.4	ND	30.2 ± 2.2	293 ± 64.5
H69	1.3	1.3	2.0	ND	56.5 ± 3.2	27.2 ± 4.1
PC-7	1.0	1.0	1.2	ND	68.8 ± 14.8	20.5 ± 8.2

The IC_{50} value (μM) of each drug was measured by MTT assay, as described in Section 2. Each value is the mean ± S.D. of three or four independent experiments.

[a] Protein expression levels were analyzed by Western blotting.

[b] Drug concentration responsible for 50% growth inhibition in MTT assay at 72 h, calculated data for at least three dependent experiments.

[c] 15-base deletion EGFR, ND: not determined.

3.2. Cellular sensitivity of lung cancer cells to gefitinib and SN-38

The growth inhibitory effect of gefitinib and SN-38 on lung cancer cells was examined using an MTT assay. The IC_{50} values of gefitinib for the cell lines ranged from 46 nM (PC-9 cells) to 68 μM (PC-7 cells). The PC-9/ZD cells were ~200-fold resistant to gefitinib, compared with the parental PC-9 cells. Cellular sensitivity to gefitinib and the expression levels of EGFR and Her2 were negatively correlated with the IC_{50} values of gefitinib (Table 1). The IC_{50} values of SN-38 for these cell lines ranged from 1 nM (SBC-3) to 300 nM (A549). The range of sensitivity to gefitinib was wider than that to SN-38. No correlation in cellular sensitivity to gefitinib and SN-38 was seen.

3.3. In vitro combined effect of gefitinib and SN-38 on lung cancer cell lines

To evaluate the potential combined effect of gefitinib and SN-38, the combination index was determined using an MTT assay. The combined effects of gefitinib and SN-38 under the concurrent schedule are shown in Fig. 1. CI values of <1, >1, and 1 indicate a supra-additive effect (synergism), an antagonistic effect, and an additive effect, respectively. An additive to supra-additive growth-inhibitory effect was observed for all doses of gefitinib and SN-38 tested in cell lines expressing wild-type EGFR. On the other hand, a high CI index was observed in PC-9 cells and PC-9/ZD cells expressing mutant EGFR over a wide range of inhibition levels. These results suggest that gefitinib and SN-38 are synergistic in lung cancer cells expressing wild-type EGFR but not in cell lines expressing mutant EGFR in vitro.

3.4. Schedule-dependent synergy of gefitinib and SN-38 in lung cancer cells

Next, we examined the schedule dependency of the combined effects of gefitinib and SN-38 in the cell lines. The five cell lines expressing wild-type EGFR showed synergistic (PC-14, H69, and A549 cells) or additive effects (SBC-3 and PC-7 cells) for all three schedules: concurrent administration, SN-38 followed by gefitinib administration, and gefitinib followed by SN-38 administration (Fig. 1A). In the PC-9 cells, concurrent administration and gefitinib followed by SN-38 administration were antagonistic, but SN-38 followed by gefitinib administration was synergistic (Fig. 1B). In the PC-9/ZD cells, concurrent administration was antagonistic, but sequential administration was synergistic. These schedule-dependent combined effects were observed in the cells expressing mutant EGFR.

3.5. Combined effects of gefitinib and SN-38 in vivo

To estimate the schedule-dependent effects in vivo, nude mice bearing tumors were treated with gefitinib and CPT-11 according to sequential or concurrent schedules (Fig. 2A). Mice bearing PC-14 tumors were treated with gefitinib and CPT-11 according to sequential or concurrent schedules. CPT-11 (50 mg/kg) alone potentially reduced the tumor size, and the combination of gefitinib and CPT-11 was synergistic. In particular, the administration of CPT-11 followed by gefitinib cured the mice bearing PC-14 cells (Fig. 2B).

Mice bearing PC-9 or PC-9/ZD tumors were treated with gefitinib and CPT-11 according to sequential or concurrent schedules. Gefitinib (40 mg/kg) alone potentially reduced the PC-9 tumors, and CPT-11 (50 mg/kg) followed by gefitinib administration reduced the tumor size of PC-9 xenografts more dramatically (gefitinib alone: $P=0.012$, sequential combination: $P=0.005$) (Fig. 2B). On the other hand, the concurrent schedule produced an antagonistic effect. Body weight loss was not observed in any of the mice treated according to the above schedules (Fig. 2C). CPT-11 followed by gefitinib administration is a potentially beneficial schedule against PC-9 and PC-9/ZD cells expressing mutational EGFR. The results of these in vivo experiments were consistent with those of the in vitro studies.

To elucidate the synergistic mechanisms of CPT-11 and gefitinib in vivo, tumor samples of the PC-9 and PC-9/ZD

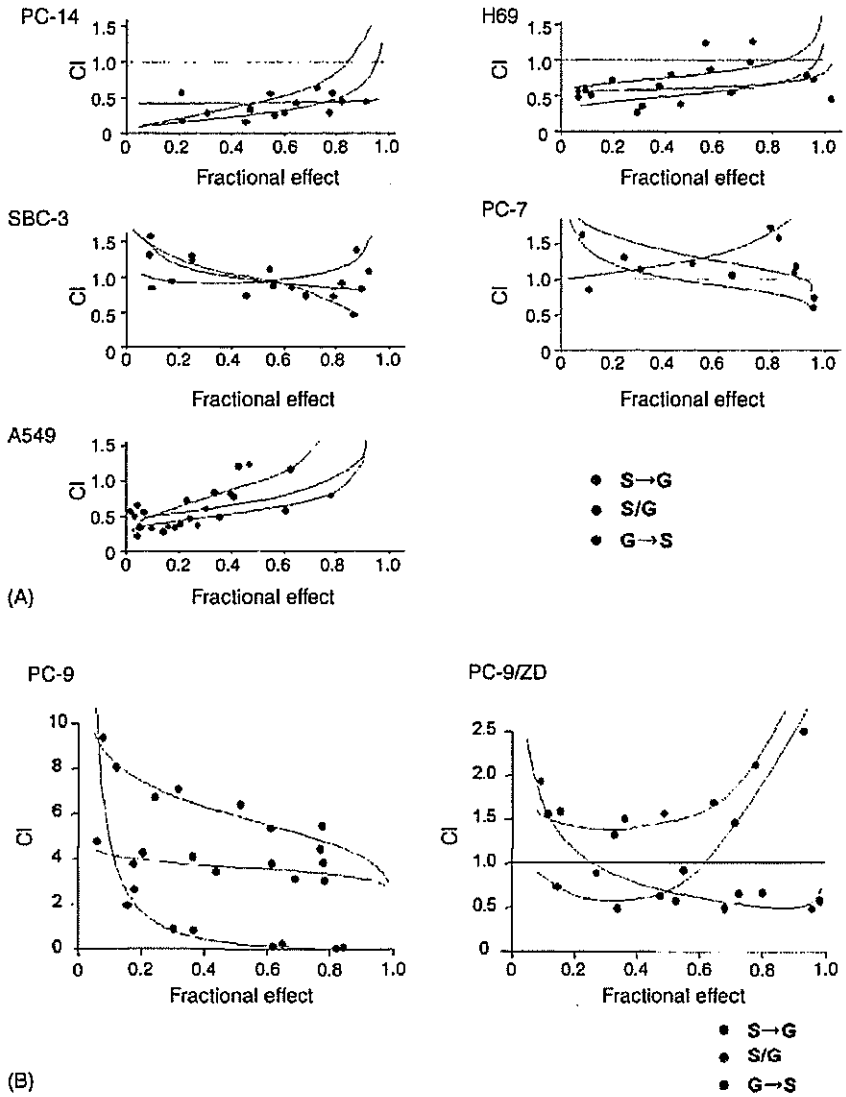

Fig. 1 Combination index (CI) plots of interactions between gefitinib and SN-38 in lung cancer cell lines. Each cell line was treated with gefitinib and SN-38, either alone or in combination at a fixed molar ratio. (A) (PC-14) gefitinib: SN-38 = 425:1; (SBC-3) 20000:1; (A549) 100:1; (H69) 2000:1; (PC-7) 3500:1. (B) (PC-9) gefitinib: SN-38 = 6:1; (PC-9ZD) 175:1. Treatment schedule: (1) SN-38 was applied first and gefitinib was applied 12 h later, followed by incubation in medium for 72 h (blue). (2) SN-8 and gefitinib were applied concurrently, followed by incubation in medium for 72 h (red). (3) Gefitinib was applied first and SN-38 was applied 12 h later, followed by incubation in medium for 72 h (green). S → G: sequential combination (SN-38 followed by gefitinib); C/G: concurrent combination; G → S: sequential combination (gefitinib followed by SN-38).

cells were stained with anti-Ki-67, anti-CD31 and the TUNEL assay (Fig. 3A and B). A reduction in tumor cell proliferation (Ki-67 staining), a reduction in tumor vasculature (CD31 staining), and an increase in tumor apoptosis (TUNEL staining) were observed in tumors treated with gefitinib alone or gefitinib and CPT-11. The administration of CPT-11 alone increased the number of Ki-67 positive tumor cells. In the PC-9 tumors, sequential treatment resulted in a 2.7-fold increase in tumor cell apoptosis and a 1.9-fold decrease in vessel staining, compared with the results obtained in tumors treated concurrently. The ratio of apoptosis:proliferation increased 1.7-fold in sequentially treated tumors compared with tumors treated with both drugs concurrently. Quantitative analysis of tumor cell proliferation and apoptosis showed a significant difference between the effects of the concurrent and sequential schedules ($P < 0.001$), but not between concurrent and gefitinib-alone ($P > 0.01$ for all comparisons, Fig. 3C). No significant difference in CD31-positive cells was observed between the control and gefitinib-alone treatments, suggesting that gefitinib exerts no remarkable anti-angiogenetic effects ($P > 0.01$, Fig. 3C). Similar findings were observed in PC-9/ZD tumors. These findings suggest that the antitumor activity of sequential treatment using gefitinib and CPT-11 is mediated by an increase in tumor cell apoptosis, compared with concurrent treatment.

4. Discussion

The EGFR-targeting drug gefitinib has been approved in many countries for the treatment of NSCLC patients who have previously received chemotherapy. Previous preclinical models have demonstrated the synergistic effects of gefitinib and platinums or taxanes [8,9]. However, no significant difference in survival was demonstrated in two randomized placebo-controlled phase II trials examining over 2000 previously untreated patients with NSCLC. In these trials, gefitinib was given in combination with paclitaxel and carboplatin or with gemcitabine and cisplatin [10,11]. Different administration schedules for gefitinib and cytotoxic agents may be necessary for select populations.

EGFR gene mutations have been demonstrated in NSCLC, and patients with lung cancers expressing mutant EGFR are strongly suspected to be hypersensitive to gefitinib alone. An in-frame short deletion in exon 19 of EGFR is strongly related to hyperresponsiveness to gefitinib and other tyrosine kinase inhibitors [12,13]. Cells expressing this deletional EGFR mutation are hypersenstivie to EGFR-targeted tyrosine kinase inhibitors [5]. On the other hand, the treat-

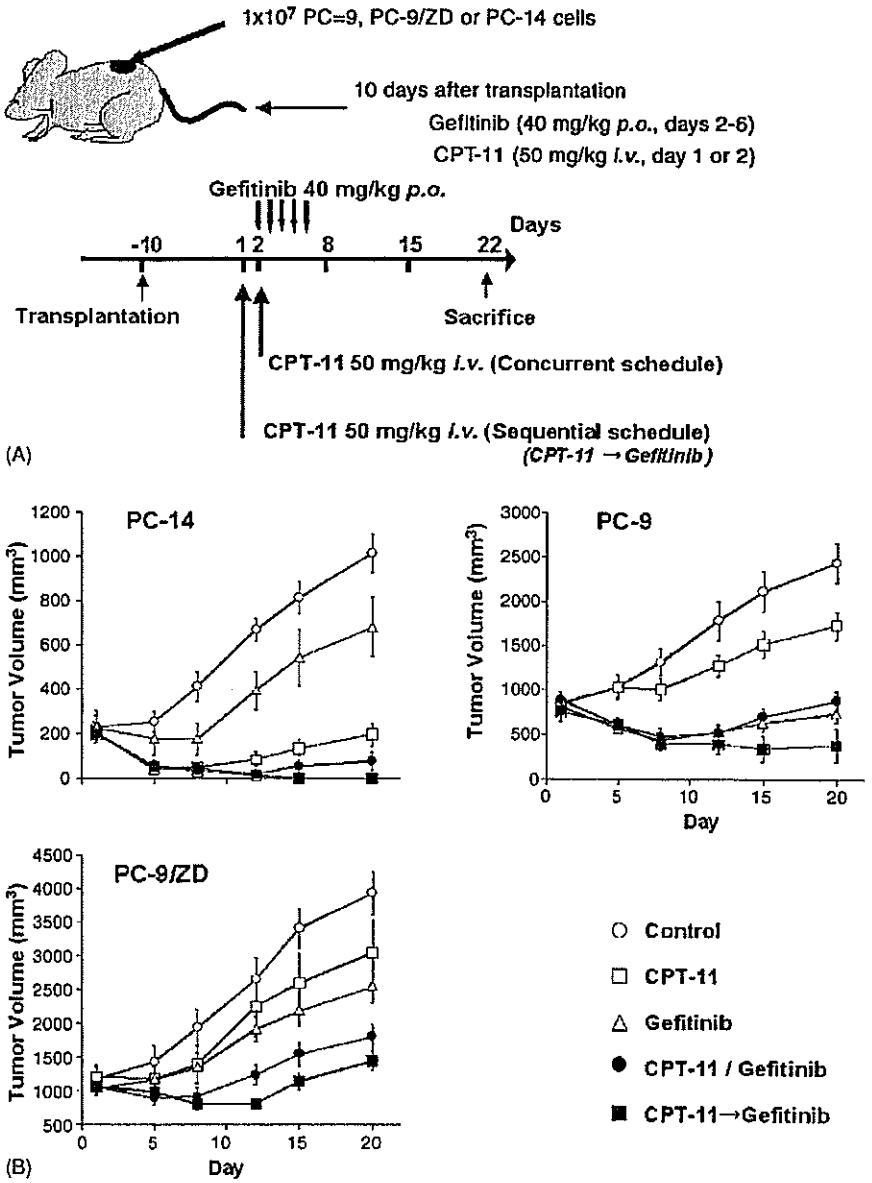

Fig. 2 Dose-dependent effects of combination therapy in PC9 and PC9/ZD cells in vivo. (A) Treatment schedule; (B) significant tumor growth-inhibition was observed in mice treated with the combination of gefitinib and CPT-11. Mice were allocated to five groups (6 mice/group) (○: 5% (w/v) glucose solution; □: CPT-11 50 mg/kg; △: gefitinib 40 mg/kg; ■: ZD1839 40 mg/kg + CPT-11 50 mg/kg concurrently; ●: CPT-11 50 mg/kg followed by ZD1839 40 mg/kg). (C) Treatment-related body weight loss in mice treated with gefitinib and/or SN-38. (○: 5% (w/v) glucose solution; □: CPT-11 50 mg/kg; △: ZD1839 40 mg/kg; ■: ZD1839 40 mg/kg + CPT-11 50 mg/kg concurrently; ●: CPT-11 50 mg/kg followed by ZD1839 40 mg/kg). Bars: ±S.D.

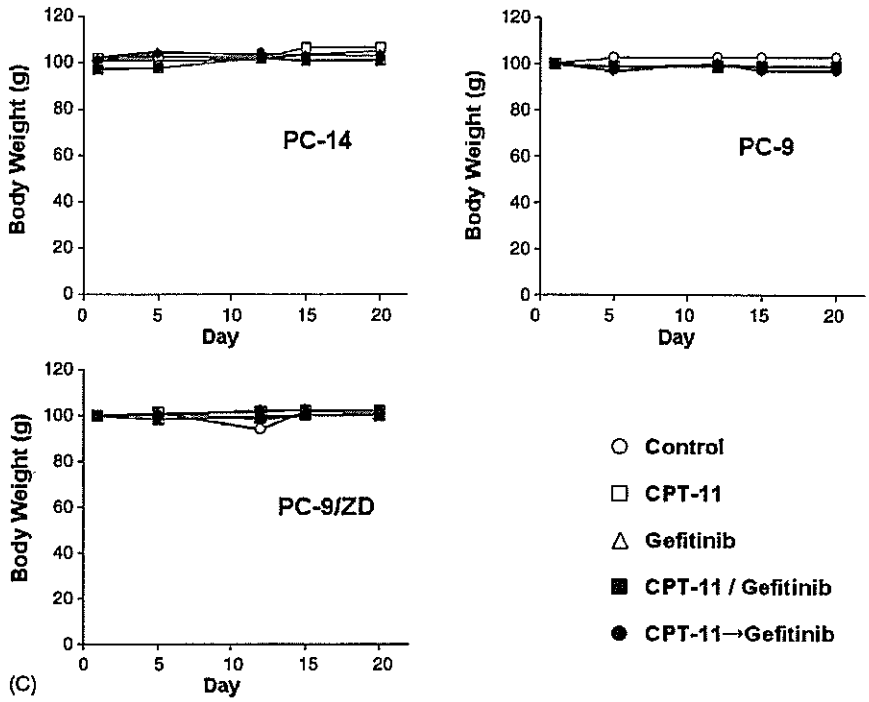

Fig. 2 (*Continued*).

ment of lung cancers expressing wild-type EGFR is a major obstacle. Combined therapies are still considered to be a major strategy against lung cancer expressing wild-type EGFR. Our previous preclinical study demonstrated that gefitinib and CPT-11 have synergistic effects in colorectal cancer cell lines [14]. Here, we reevaluated the combined effects of gefitinib and cytotoxic agents based on the status of EGFR mutations in lung cancer.

We demonstrated that gefitinib and SN-38, the active form of CPT-11, have synergistic or additive effects in lung cancer cells expressing wild-type EGFR. The combination of gefitinib and CPT-11 may be useful against lung cancers expressing wild-type EGFR. On the other hand, this combination had antagonistic effects in PC-9 cells expressing mutant EGFR, even though PC-9 cells are basically hypersensitive to gefitinib alone.

The concurrent administration of gefitinib and SN-38 also had an antagonistic effect in the PC-9/ZD cells. The PC-9/ZD cells developed an acquired resistance to gefitinib after exposure to gefitinib in vitro. New treatment strategies for patients who are refractory to gefitinib treatment are clinically needed. We demonstrated that the sequential administration of SN-38 (CPT-11) and gefitinib improved the combined effects in PC-9/ZD cells both in vitro and in vivo.

The above results led us to propose a combined gefitinib and CPT-11 treatment strategy based on the EGFR mutation status of lung cancers: (1) combined treatment according to any schedule for lung cancers expressing wild-type EGFR, (2) gefitinib treatment alone for lung cancers expressing mutant EGFR, and (3) the sequential administration of gefitinib and CPT-11 for patients who are refractory to gefitinib treatment. Based on the above preclinical evidence, we are preparing to begin a clinical phase II trial for combined gefitinib and CPT-11 treatment in Japan.

We previously demonstrated that CPT-11 and gefitinib have a synergistic effect against colorectal cancer [14]. EGFR mutations are rarely observed in colorectal cancer cells [15]. Therefore, the combined effects of these agents against colorectal cancers were consistent with those against the lung cancers expressing wild-type EGFR in this study.

Different combined effects were observed for the concurrent and sequential schedules in vitro and in vivo. While the mechanisms responsible for the combined effects remain unclear, cell cycle distributions might explain some of the differences. In cells treated according to the sequential gefitinib followed by SN-38 (CPT-11) treatment schedule, treatment with gefitinib resulted in an increase in the G0–G1 phase and a decrease in the S phase populations (data not shown). The decreased S phase population was not sensitive to CPT-11 [16]. Thus, the antagonistic effects of the sequential administration of gefitinib followed by CPT-11 (SN-38) could be explained by this mechanism. On the other hand, in cells treated according to the sequential SN-38 followed by gefitinib treatment schedule, SN-38 treatment induced an increase in the S phase population. If the S phase population is sensitive to gefitinib, this might explain the synergistic effects of this sequential schedule [17]. An increase in EGFR phosphorylation induced by CPT-11 is another previously reported possible mechanism responsible for this synergistic action [14].

In conclusion, we demonstrated the different effect on lung cancer cell expressing mutant EGFR according to the

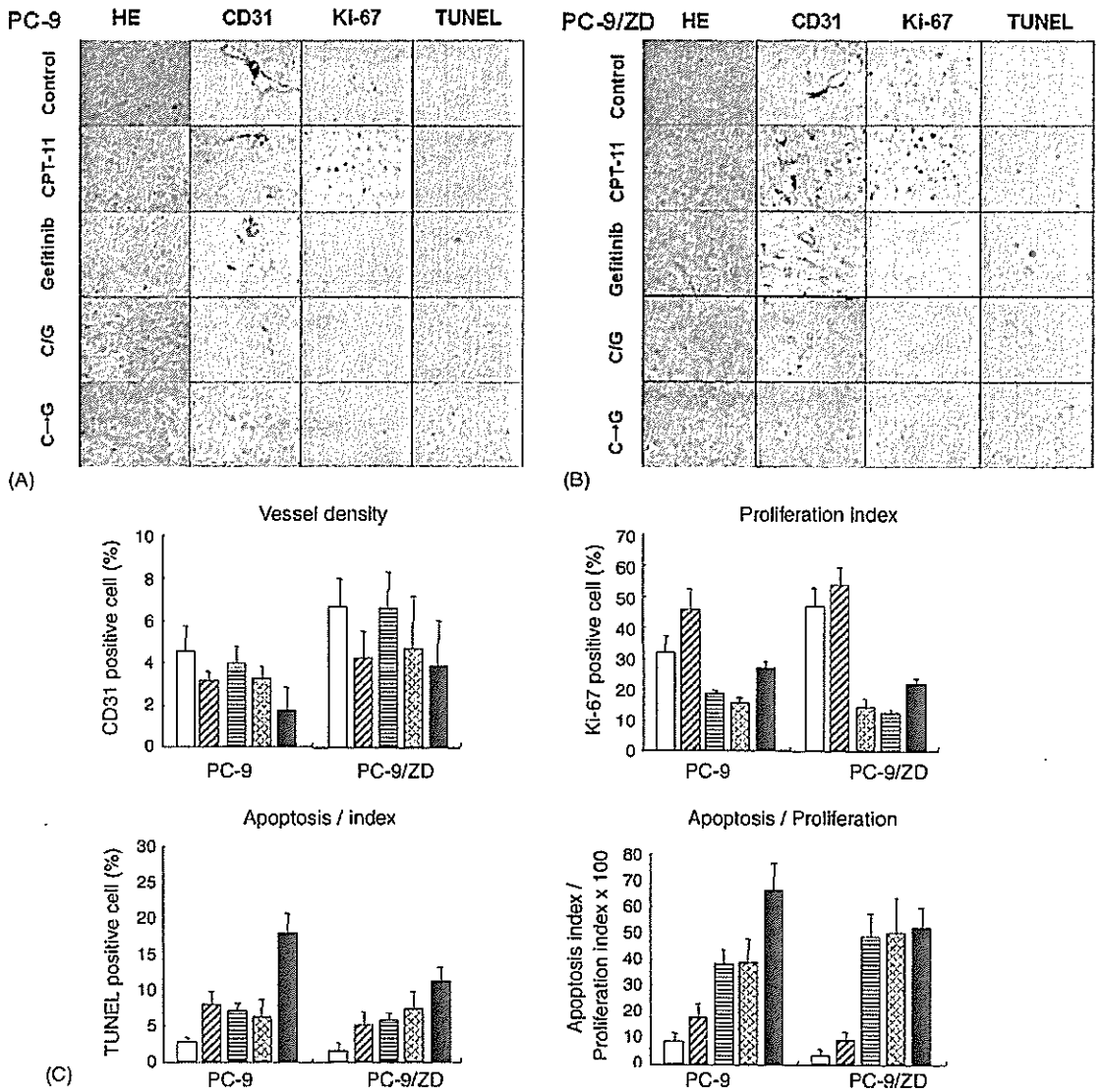

Fig. 3 (A) Historical examination of PC-9 tumor xenografts (day 22) stained with H&E, anti-CD31 vessel staining, TUNEL staining (magnification: 400×) and anti-Ki-67 nuclear antigen (magnification: 200×). The number of Ki-67-positive cells increased with the administration of CPT-11. The number of Ki-67-positive cells decreased with the gefitinib-alone and combination treatments. C/G: concurrent combination, C→G: sequential combination. (B) Historical examination of PC-9ZD tumor xenografts (day 22) stained with H&E, anti-CD31 vessel staining, TUNEL staining (magnification: 400×) and anti-Ki-67 nuclear antigen (magnification: 200×). The number of Ki-67-positive cells increased with the administration of CPT-11. The number of Ki-67-positive cells decreased with the gefitinib-alone and combination treatments. C→G: sequential combination; C/G: concurrent combination. (C) Quantitation of CD31 vessel staining, Ki-67 proliferation index, apoptosis index, and apoptosis: proliferation ratio. The columns represent the mean population of positive cells in five fields. Bars: ±S.D. Tumors from mice treated with vehicle (white), CPT-11 (diagonal hatched), Gefitinib (horizontal hatched), concurrent combination of CPT-11 plus Gefitinib (cross-hatched), or sequential combination of CPT-11 plus Gefitinib (cross-hatched).

combination schedule of gefitinib and CPT-11. The sequential combined treatment also active against lung cancer cell expressing wild-type EGFR.

Acknowledgements

This study was supported in part by a Grant-in-Aid for Cancer Research and the 3rd Term Comprehensive 10-Year Strategy for Cancer Control from the Ministry of Health, Labour and Welfare, Tokyo, Japan.

References

[1] Lynch TJ, Bell DW, Sordella R, Gurubhagavatula S, Okimoto RA, Brannigan BW, et al. Activating mutations in the epidermal growth factor receptor underlying responsiveness of non-small-